Article

Current Biology

Ongoing habenular activity is driven by forebrain networks and modulated by olfactory stimuli

Graphical abstract

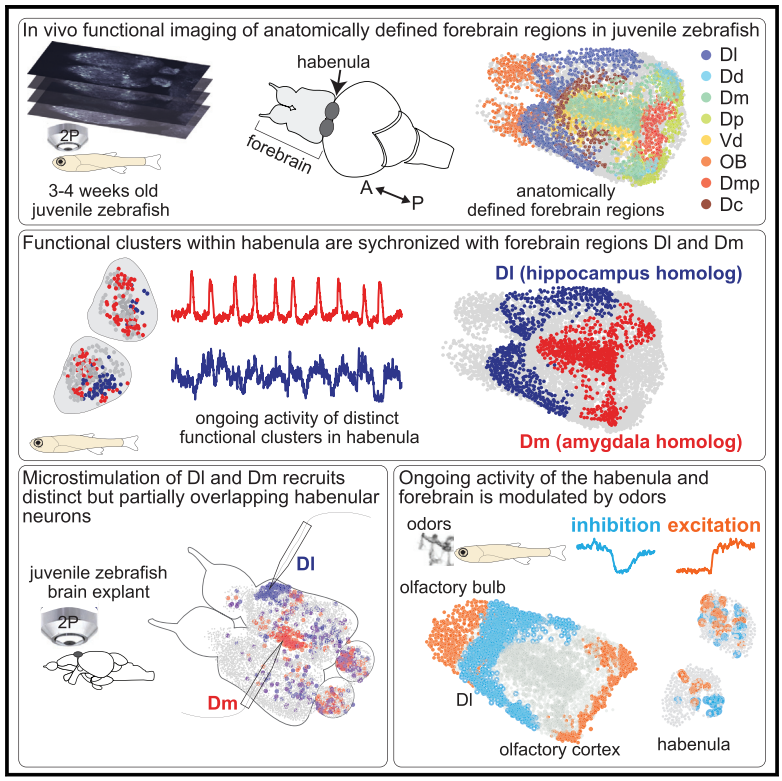

Highlights

- Ongoing habenular activity is structured into robust functional clusters
- Amygdala and hippocampus homologs in zebrafish drive ongoing habenular activity
- Activating amygdala and hippocampus recruits partially overlapping habenula neurons
- Odors modulate the activity of habenula and its forebrain input regions

Authors

Ewelina Magdalena Bartoszek, Anna Maria Ostenrath, Suresh Kumar Jetti, Bram Serneels, Aytac Kadir Mutlu, Khac Thanh Phong Chau, Emre Yaksi

Correspondence

emre.yaksi@ntnu.no

In brief

Bartoszek et al. showed that ongoing habenular activity is driven by the ancestral homologs of amygdala (Dm) and hippocampus (Dl) in zebrafish forebrain. Activating Dm and Dl recruits a partially overlapping set of habenular neurons. Odor stimulation modulates the ongoing activity and communication between forebrain networks and the habenula.

Bartoszek et al., 2021, Current Biology *31*, 3861–3874
September 13, 2021
https://doi.org/10.1016/j.cub.2021.08.021

CellPress

Current Biology

CellPress
OPEN ACCESS

Article

Ongoing habenular activity is driven by forebrain networks and modulated by olfactory stimuli

Ewelina Magdalena Bartoszek,[1] Anna Maria Ostenrath,[1,3] Suresh Kumar Jetti,[2,3] Bram Serneels,[1] Aytac Kadir Mutlu,[1] Khac Thanh Phong Chau,[1] and Emre Yaksi[1,2,4,*]

[1]Kavli Institute for Systems Neuroscience and Centre for Neural Computation, Faculty of Medicine and Health Sciences, Norwegian University of Science and Technology, Olav Kyrres gata 9, 7030 Trondheim, Norway

[2]Neuro-Electronics Research Flanders, Kapeldreef 75, 3001 Leuven, Belgium

[3]These authors contributed equally

[4]Lead contact

*Correspondence: emre.yaksi@ntnu.no

https://doi.org/10.1016/j.cub.2021.08.021

SUMMARY

Ongoing neural activity, which represents internal brain states, is constantly modulated by the sensory information that is generated by the environment. In this study, we show that the habenular circuits act as a major brain hub integrating the structured ongoing activity of the limbic forebrain circuitry and the olfactory information. We demonstrate that ancestral homologs of amygdala and hippocampus in zebrafish forebrain are the major drivers of ongoing habenular activity. We also reveal that odor stimuli can modulate the activity of specific habenular neurons that are driven by this forebrain circuitry. Our results highlight a major role for the olfactory system in regulating the ongoing activity of the habenula and the forebrain, thereby altering brain's internal states.

INTRODUCTION

Continuous interactions between the sensory world and the internal states of the brain are essential for survival. For example, a sudden change in the environment by the presence of a salient sensory cue can be critical for updating an animal's brain from its resting to an alert state.[1,2] Seminal studies in human subjects clearly demonstrated the presence of such rapid alterations from a default state with high levels of brain activity[3] to an alert state with reduced levels of global network activity and increased activity in sensory or attention-related areas during various tasks.[2,4,5] While the precise definition of a "brain state" can vary depending on the timescales of investigated phenomena, the link between ongoing (or spontaneous) brain activity and the current state of the brain is well accepted.[6–8] In fact, ongoing neural activity has been observed across the nervous system, from brain areas involved in sensory processing,[9–12] to innate behaviors[13] and higher cognitive function.[14–16] Despite the presence of ongoing activity across the brain and its rapid alterations coupled with brain state transitions, dedicated neural pathways and their connection to ongoing brain activity and sensory-evoked transitions remain to be identified.

One brain region that receives information from both sensory[17–19] and cortico-limbic[20–31] brain structures, and exhibits a high level of ongoing neural activity, is the habenula. This evolutionarily conserved diencephalic nucleus[22,32,33] is a major hub relaying information from diverse forebrain inputs[20–26,28,34] to its target regions that directly control animal behavior via the release of dopamine, acetylcholine, and serotonin.[19,22,23,35–38] Previous studies established a direct role for the habenula in adaptive behaviors,[6,36,37,39–43] learning,[23,25,36,42,44,45] and prediction of outcomes.[23,40,44,46] Not surprisingly, habenular dysfunction is closely linked to several neurological conditions and mood disorders including depression.[31,47,48] Based on molecular profiles,[49–51] anatomical landmarks,[36,42,45,52] and neural activity,[29,30,36,53] habenula is divided into numerous subdomains. Most prominent in zebrafish are the dorsal (dHb) and the ventral habenula (vHb), which are homologous to mammalian medial and lateral habenula,[36,42,45,52] respectively. dHb is involved in sensory processing,[19,30,38,53] circadian rhythms,[38] social behaviors,[41] and experience-dependent fear response,[37,42,45] whereas vHb plays important roles in learning[36] and active coping behavior.[6] Recent studies showed that ongoing neural activity associated with the transition between brain states is present in both dHb and vHb.[6,29,30,37] Interestingly, sensory cues that have been shown to induce prominent behavioral responses in zebrafish[6,37,51,54] were also shown to elicit distinct neural responses both in dHb[18,29,37,53] and vHb.[6,29] Yet it is less clear how ongoing habenular activity is generated by the distributed brain networks and how this ongoing activity interacts with sensory responses in the habenula and across the brain.

In this study, we investigated how interactions between ongoing and sensory-evoked activity can shape brain's internal states, in the habenula and across the entire zebrafish forebrain. First, we showed that functional interactions of neurons within distinct habenular subdomains are stable and spatially organized across different periods of ongoing activity. Next, we revealed that ongoing habenular activity is driven by the ancestral homologs of limbic forebrain regions, hippocampus (Dl) and amygdala (Dm). Finally, we demonstrated that olfactory cues modulate the internally generated ongoing activity of habenular neurons driven by ancestral limbic forebrain regions. Our results

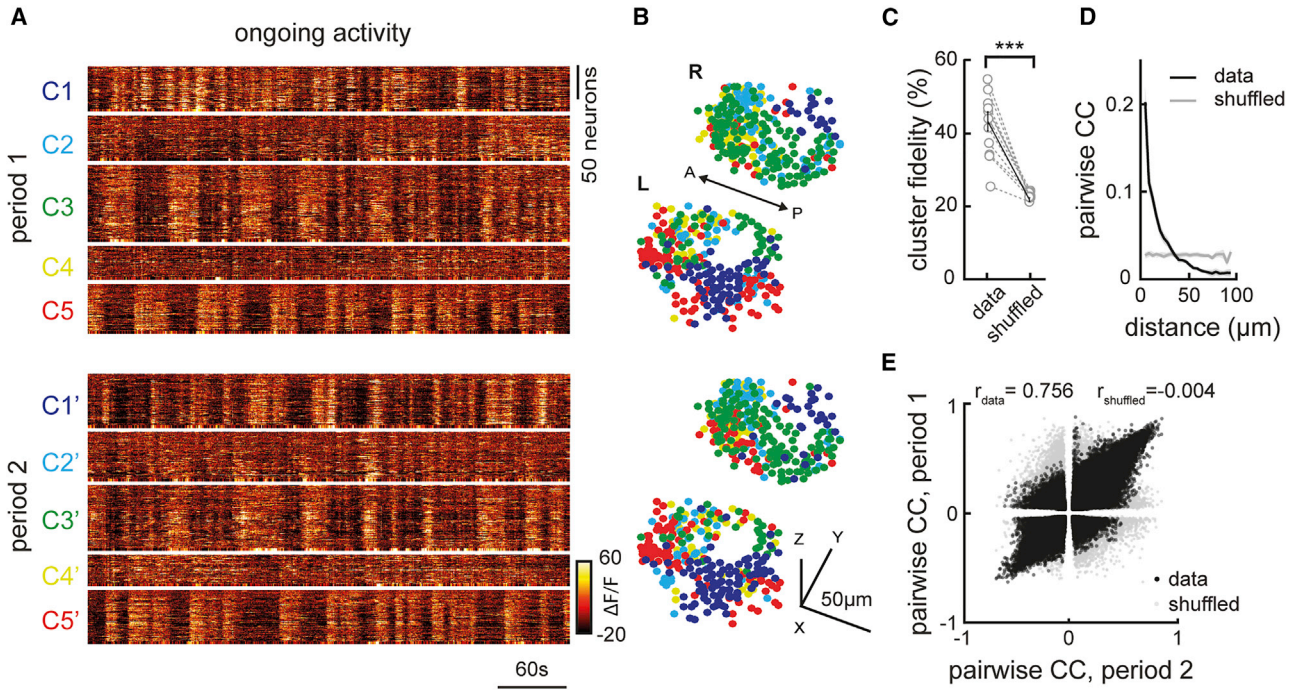

Figure 1. Ongoing activity of habenular neurons is temporally and spatially organized

(A) Representative example of ongoing habenular activity recorded by two-photon calcium imaging in *Tg(eval3:GCaMP6s)* zebrafish line. Habenular neurons are clustered (C1–5) using k-means clustering over two consecutive time periods of 7 min each (period 1, top; period 2, bottom). Warm colors represent higher calcium signals.

(B) Representative example of three-dimensional reconstruction of habenular neurons clustered using k-means clustering in two consecutive time periods (top and bottom). Neurons are color-coded based on their cluster identity that corresponds to the calcium signals depicted in (A). L, left; R, right hemisphere; A, anterior; P, posterior.

(C) The ratio of habenular neuron pairs remaining in the same functional clusters (high cluster fidelity) is significantly higher than chance levels during two different time periods of ongoing activity. 315 ± 35 (mean ± SEM) habenular neurons were imaged in each fish (n = 11 fish). ***p < 0.001, Wilcoxon signed-rank test.

(D) Relation between pairwise correlation of habenular neurons during ongoing activity and the distance between each neuron pair. Gray line represents shuffled spatial distributions.

(E) Pairwise correlations of calcium traces of habenular neurons ($p < 0.05$) during two consecutive time periods, in black. Gray dots represent pairwise comparison shuffled for pair identities. Actual data exhibit a correlation of $r_{data} = 0.756$ for the pairwise correlation across two time periods, indicating robust synchrony between pairs of neurons. Shuffled distribution is $r_s = -0.004$.

See also Figure S1.

reveal that the habenula acts as a hub integrating limbic and sensory signals, and olfactory cues switch internal brain states by inhibiting the ongoing activity of the habenula and its ancestral limbic forebrain inputs.

RESULTS

Structured ongoing activity in the habenula is stable over time

To investigate ongoing habenular activity, we performed volumetric two-photon calcium imaging across the entire habenula of juvenile *Tg(elavl3:GCaMP6s)* zebrafish,[29,55–57] expressing GCaMP6s pan-neuronally. In all our experiments, we used 3- to 4-week-old zebrafish[58] that were shown to exhibit complex behaviors such as learning[44,59–61] and social interactions,[62,63] which are mediated by habenular circuits.[36,41,42,44,46] We observed structured ongoing activity across the entire habenula (Figure 1A), in line with earlier studies focusing on the dHb.[30] To quantify ongoing habenular activity, we performed k-means clustering of habenular calcium signals. We observed that distinct functional clusters of habenular neurons exhibit synchronous activity (Figures 1A, 1B, and S1A), which can optimally be represented by around 5–6 clusters based on elbow test (Figures S1B and S1C). Next, we investigated whether such functional clusters in habenula are stable across different time periods by comparing the activity of functional clusters that were recorded in two consecutive time windows. We quantified the stability of habenular clusters by measuring the probability of a pair of habenular neurons in the same cluster during period #1 (Figure 1A, top) to remain in the same clusters in period #2 (Figure 1A, bottom), which we termed "cluster fidelity."[29,30] We observed that more than 40% of habenular neuron pairs remained in the same cluster, which is significantly above chance levels (Figure 1C). Moreover, functional clusters of habenula remained stable (significantly above chance levels) across a range of different time windows (Figure S1D) and with various selected number of clusters (Figure S1E). Clusters of habenular neurons appeared to be spatially organized (Figures 1B and S1). To quantify the spatial distribution of the synchronous habenular activity, we plot the average pairwise correlation of neurons versus the

distance between them. We observed that nearby habenular neurons exhibit more correlated/synchronous ongoing activity, when compared to distant pairs of neurons within each habenular hemisphere (Figure 1D). Our results using k-means clustering of ongoing habenular activity suggest that while neurons within the same clusters exhibit highly correlated activity (i.e., within individual clusters of Figure 1A), neurons in different clusters can also be anti-correlated (i.e., between cluster #3 and cluster #5 of Figure 1A). We investigated whether such correlations and anti-correlations between habenular neurons are stable across different time periods by plotting pairwise correlations of all recorded neuron pairs. In fact, we observed that correlations and anti-correlations between habenular neurons remained stable across different time periods (Figure 1E, black), and this relationship was different from shuffled distributions of such pairwise relationships (Figure 1E, gray). Our findings on functional clustering and correlations of ongoing habenular activity also remained consistent with deconvolved calcium traces (Figures S1F–S1I). Taken together, these results revealed that the ongoing habenular activity is highly structured, stable over time, and spatially organized into functional clusters of habenular neurons exhibiting synchronous or anti-synchronous ongoing activity.

Distinct forebrain regions correlate with ongoing habenular activity

Previous studies in mammals[23,25,26,28,64,65] and zebrafish[18,20,29,30,37,38,41,42,44,49,53] showed that several forebrain regions send anatomical projections to the habenula. We asked which of these candidate forebrain regions might drive or modulate ongoing habenular activity. To address this question, we measured the ongoing activity of the entire forebrain of the juvenile zebrafish, including the habenula, by using volumetric two-photon calcium imaging. To identify forebrain regions that might drive distinct functional clusters of habenula, we asked which forebrain neurons are highly correlated with the average ongoing activity of individual habenular clusters (Figures 2A and 2B). We observed that the neurons of dorsolateral (Dl), dorsomedial (Dm), ventrodorsal forebrain (Vd), and the olfactory bulbs (OB) contained neurons with highest correlations to individual habenular clusters (Figures 2C, 2D, S2A, and S2B).

To identify and quantify the forebrain regions driving habenula, we manually delineated distinct forebrain nuclei using anatomical landmarks that were identified by previous studies in zebrafish[17,66–72] and in other teleosts[73–77] (Figures 2E and 2F). To further test whether anatomically identified forebrain regions overlapped with functionally distinct forebrain clusters, we compared those manually delineated forebrain nuclei (Figures S2A and S2B) with k-means functional clusters of ongoing forebrain activity (Figures S2C–S2E). We quantified this overlap with a previously used cluster selectivity index.[29,30] Cluster selectivity would be "0" if all neurons of anatomically delineated nuclei were randomly distributed to different functional clusters, or "1" if all neurons of the nuclei were in the same functional cluster. In fact, our results showed that cluster selectivity is significantly higher than the chance levels for all forebrain regions (Figure S2F), suggesting that the neurons of manually delineated forebrain regions are selective to one or few functional clusters. Next, we asked in which of these forebrain regions we can find neurons that are strongly correlated (Pearson's correlation above 0.1) with the average ongoing activity of each habenular cluster. Our results revealed that the Dl, Dm, and Vd telencephalic regions, homologous to mammalian hippocampus,[76–80] amygdala,[68,73,78,79,81] and striatum,[32,78] respectively, contain the largest fraction of habenula correlated neurons, in addition to the olfactory pathway (Figures 2G and S1I). These results suggest that ancestral homologs of mammalian limbic forebrain circuits in zebrafish, Dl, Dm, Vd, are potential candidates to drive ongoing habenular activity.

Next, we asked whether different sub-circuits of zebrafish habenula might exhibit correlated activity with distinct forebrain regions. To achieve this, we first identified functional habenular clusters corresponding to dHb and vHb,[36,42,45,52] based on the spatial location of these functional clusters in the habenula (Figure S3A, red for dorsal and blue for ventral clusters). Subsequently, we quantified how the ongoing activity of these specific functional clusters located in ventral versus dorsal habenula relates to the ongoing activity of distinct forebrain regions. Our results revealed that while the habenular neurons of ventral functional clusters are correlated with significantly more neurons in Dl, dorsal functional clusters of the habenula are correlated with significantly more neurons in Dm and OB (Figure S3B). To verify these results further, we performed dual-channel calcium recordings of *Tg(elavl3:GCaMP6s)* zebrafish that also express red fluorophore mCherry in vHb (*Tg(dao:GAL4VP16; UAS-E1b:NTR-mCherry)*)[36] and dHb (*Tg(narp:GAL4VP16; UAS-E1b:NTR-mCherry)*).[42] We observed that *Tg(dao:GAL4VP16)* labels 20% of habenular neurons located in vHb (Figure S3C, blue). Moreover, we showed that average vHb activity correlates with spatially organized forebrain neurons (Figure S3C, warm colors), with a significantly higher preference for Dl and significantly less preference for Dm and OB (Figure S3D), when compared to random habenular neurons. We also observed that *Tg(narp:GAL4VP16)* labels on average 68% of Hb neurons in juvenile zebrafish (Figure S3E, red) and is, therefore, too broad to be used as a specific genetic marker for dlHb neurons, unlike adult zebrafish.[42] As a result, we saw that *Tg(narp:GAL4VP16)*-labeled neurons showed preference similar to general distributions of forebrain correlations of random habenular neurons (Figures S3E and S3F), except the significant preference for OB. This data revealed that despite largely overlapping correlation preferences across habenula, the functional clusters corresponding to ventral zones of the habenula exhibit a significantly higher tendency to correlate with Dl neurons, while the functional clusters located in dorsal zones of the habenula prefer to correlate with Dm and OB.

Electrical micro-stimulation of limbic forebrain regions Dl and Dm elicits spatially organized responses in the habenula

Our correlation-based functional connectivity measurements (Figure 2) suggest that distinct limbic forebrain regions might be the major drivers of ongoing habenular activity. To test this hypothesis directly, we locally activated dorsal forebrain by a glass micro-stimulation electrode while measuring forebrain and habenular activity in a juvenile zebrafish brain-explant preparation with intact connectivity.[56] Inserting the micro-stimulation electrode in Dl or Dm allowed direct activation of a large fraction of these dorsal forebrain regions (Figures 3A and 3J). Micro-stimulation of Dl and Dm elicit significant activation in 23%–29% of

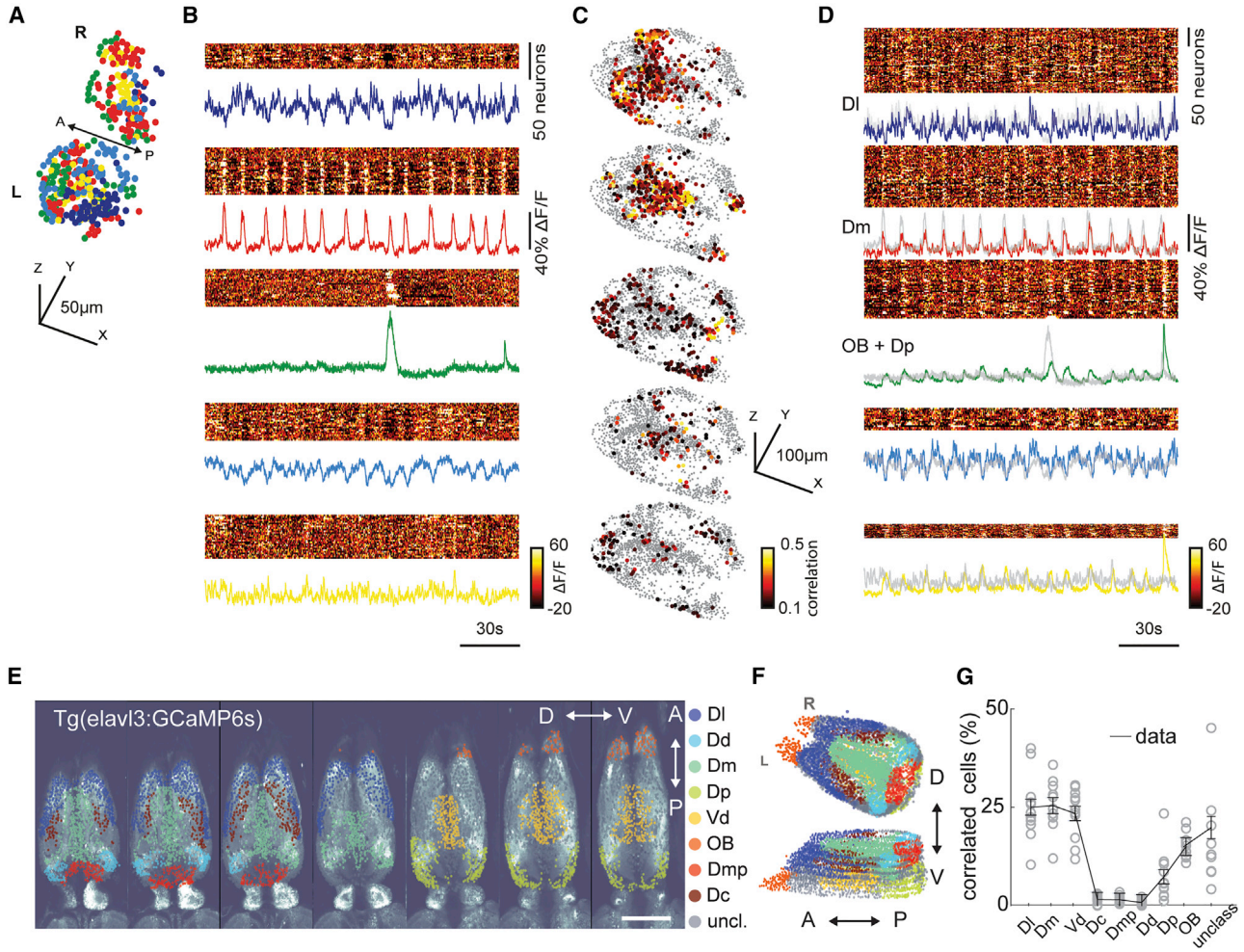

Figure 2. Ongoing activity of habenular neurons is correlated with sensory and limbic forebrain regions

(A) Three-dimensional reconstruction of habenular neurons detected in *Tg(elavl3:GCaMP6s)* zebrafish line, clustered with k-means clustering. Colors represent neural clusters with similar ongoing activity. L, left; R, right hemisphere. 315 ± 35 (mean ± SEM) habenular neurons were imaged in each fish (n = 11 fish).

(B) Ongoing activity of the habenular neurons corresponding to clusters in (A). Warm colors represent higher neural activity. Color-coded traces represent the average activity of all neurons in each cluster.

(C) Three-dimensional reconstruction of forebrain neurons that are strongly correlated (Pearson's correlation > 0.1) to average ongoing activity of different habenular clusters in (B). Warm colors represent stronger correlations. 2,135 ± 345 (mean ± SEM) forebrain neurons were imaged in each fish (n = 11 fish).

(D) Ongoing activity of the forebrain neurons corresponding to clusters of neurons depicted in (C). Color-coded traces represent the average activity of neurons in each cluster. Gray traces represent the average activity of habenular clusters in (B). Note that the ongoing activity of identified forebrain neurons and habenular clusters is highly similar.

(E) Forebrain regions identified based on anatomical landmarks are color coded and overlaid on raw two-photon microscopy image. Scale bar represents 100 μm. Optical planes are shown from dorsal to ventral. A, anterior; P, posterior; D, dorsal; V, ventral.

(F) Three-dimensional reconstruction of forebrain regions shown in (E).

(G) Distribution of forebrain neurons with strong correlation (>0.1) to ongoing habenular activity into anatomically identified forebrain regions. Dl, dorsolateral telencephalon; Dd, dorsal nucleus of the dorsal telencephalon; Dm, dorsomedial telencephalon; Dp, posterior zone of the dorsal telencephalon; Vd, dorsal nucleus of the ventral telencephalon; OB, olfactory bulb; Dmp, posterior nucleus of dorsomedial telencephalon; Dc, central zone of the dorsal telencephalon; unclass, unclassified. Black lines represent mean ± SEM (n = 11 fish). Each fish is presented as an open circle. Number of neurons detected in each brain region: Dl, 230 ± 35; Dd, 55 ± 9; Dm, 213 ± 33; Dp, 155 ± 24; Vd, 260 ± 40; OB, 273 ± 42; Dmp, 76 ± 12; Dc, 111 ± 17; unclassified, 774 ± 120; mean ± SEM.

See also Figures S1–S3.

habenular neurons (Figures 3B, 3C, 3K, and 3L) that are spatially organized (Figures 3D and 3M). Due to its intact connectivity, juvenile zebrafish brain explant exhibits ongoing habenular activity with a similar number of calcium bursts when compared to our *in vivo* recordings (Figure S4R). This ongoing activity in brain explants has sufficient structure that allowed us to identify functional clusters in habenula by using k-means clustering (Figures 3E, 3F, 3N, and 3O). We observed that ~40% of habenular neurons (significantly higher than chance levels) within a given functional cluster remained in the same cluster during forebrain micro-stimulation of Dm and Dl (Figures 3G–3I and 3P–3R). These results revealed a causal relationship between stimulation

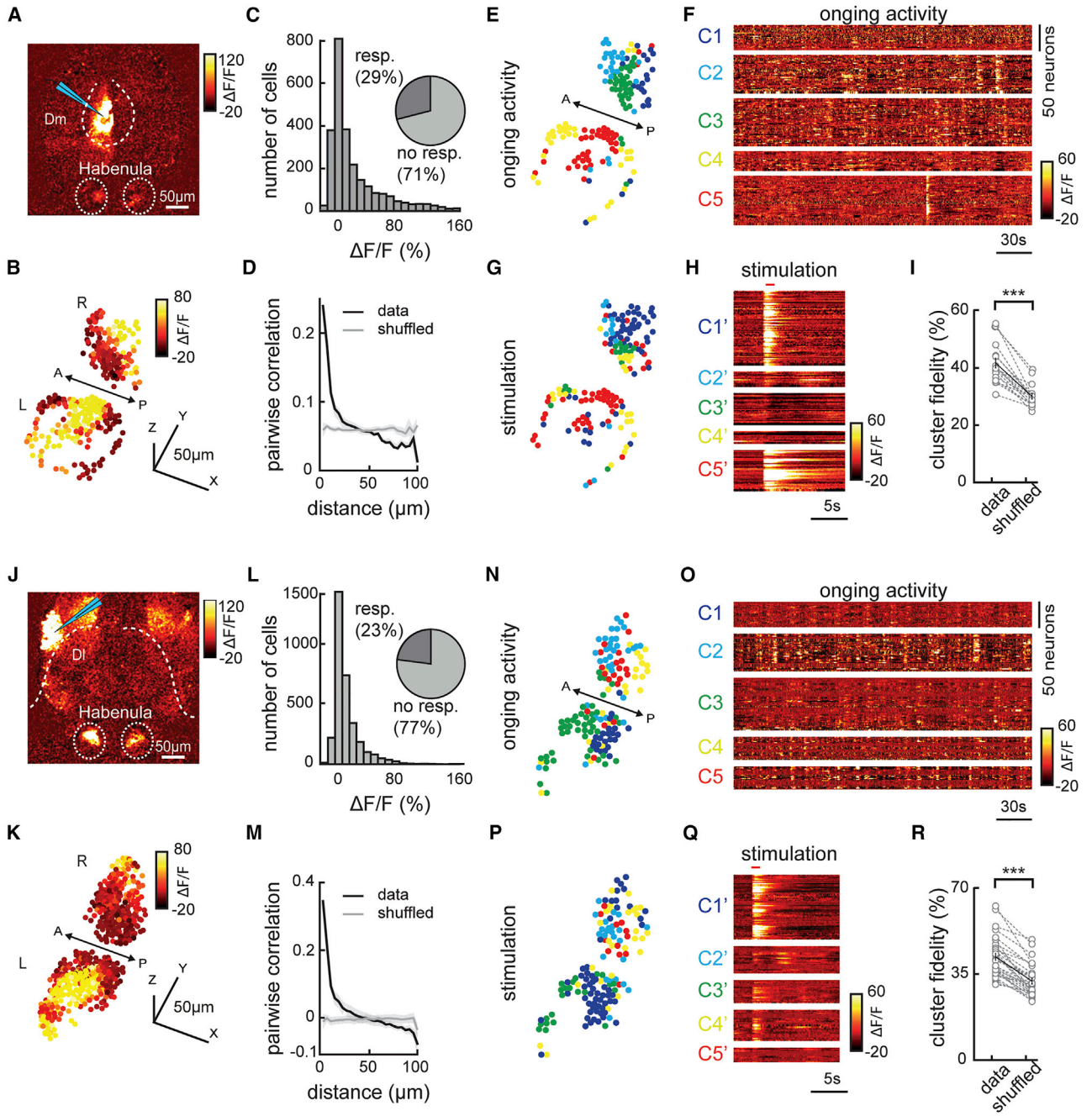

Figure 3. Electrical micro-stimulation of forebrain regions Dm and DI activates spatially organized clusters of habenular neurons

(A) Two-photon calcium signals upon electrical micro-stimulation of forebrain region Dm in *Tg(eval3:GCaMP5)* juvenile zebrafish brain explant. Warm colors represent stronger neural activity. Cyan triangle represents electrode location. Habenula and Dm are delineated with dashed lines.

(B) Reconstruction of habenular responses upon Dm micro-stimulation.

(C) Histogram representing the responses of habenular neurons upon Dm micro-stimulation (511 ± 72 neurons per fish, in n = 5 fish). Pie chart represents the ratio of habenular neurons that are activated 2 SDs higher than baseline levels upon Dm micro-stimulation.

(D) Relation between pairwise correlation of habenular neuron responses upon Dm micro-stimulation and the distance between each neuron pair. Gray line represents shuffled spatial distribution.

(E) Reconstruction of habenular neurons clustered with k-means functional clustering of their ongoing activity in juvenile zebrafish brain explant. Colors represent habenular clusters with similar ongoing activity. Scale bar represents 50 μm. L, left; R, right hemisphere.

(F) Ongoing activity of the habenular neurons corresponding to clusters in (E).

(G) Reconstruction of habenular neurons clustered during Dm micro-stimulation using k-means clustering. Colors represent habenular clusters with similar responses to Dm micro-stimulation. L, left; R, right hemisphere.

(legend continued on next page)

of forebrain regions Dm and Dl with the activation of habenular neurons, thereby confirming functional connections from these ancestral limbic dorsal forebrain structures onto the habenula. Our results also demonstrated that structured ongoing activity of habenula carries information from its input regions in the forebrain.

To further investigate how distinct forebrain inputs are integrated in the habenula, we placed two micro-stimulation electrodes simultaneously in Dm and Dl regions of the same juvenile zebrafish brain explant and sequentially activated these regions while imaging the entire forebrain of *Tg(elavl3:GCaMP6s-nuclear)* zebrafish.[57] We observed that Dm and Dl activation recruited a partially overlapping, but distinct set of habenular neurons (Figures 4A and 4B). Despite the micro-stimulation of similar proportion neurons in Dm and Dl (Figure S4P), we observed that stimulating Dm recruits a significantly higher ratio of forebrain responsive habenular neurons when compared to Dl stimulation (Figure 4C). We also observed that Dm stimulation recruits a significantly larger number of habenular neurons in the ipsilateral hemisphere (red labels in Figures 4D and S4A–S4I), whereas Dl stimulation elicited similar responses in both ipsi- and contralateral habenula (blue labels in Figures 4D and S4A–S4I). These results suggest that functional inputs originating from Dm and Dl might go through different pathways before they reach partially overlapping populations of habenular neurons.

Last, to confirm the specificity of our forebrain activation, we choose to place our micro-stimulation electrode on the forebrain region near Dp and Dmp, which are spatially close to habenula, but without any known functional connections to habenula. In fact, while micro-stimulation in the Dp/Dmp region elicits activity in a similar ratio of neurons in the stimulated region when compared to Dm or Dl (Figure S4P), we observed that activating this control Dp/Dmp region did not elicit activity significantly more than the ongoing activity of the habenula, unlike activating Dm and Dl regions (Figure S4Q). We also showed that application of glutamate receptor blockers (AP5/NBQX) silenced habenular responses (Figures S4S and S4T), confirming that the habenular responses upon forebrain micro-stimulation are not due to direct electrical activation of habenula, but due to glutamatergic inputs received by the habenular neurons.

Sensory information and limbic dorsal forebrain inputs are integrated in the habenula

Previous studies showed that habenular neurons receive direct inputs from the olfactory bulbs[17,70] and exhibit prominent chemosensory responses to diverse odors.[18,30,53] Our functional connectivity analysis (Figures 2 and S3) and forebrain micro-stimulation experiments (Figures 3 and 4) also showed that at least a part of the ongoing habenular activity is generated by the activity of the olfactory pathway and the limbic forebrain regions Dm and Dl. We asked how these chemosensory and non-sensory forebrain inputs are integrated at the level of habenula. To do this, we relied on our brain-explant preparation of juvenile zebrafish, in which the noses were kept attached, allowing micro-electrode stimulation of limbic dorsal forebrain regions, while delivering odors to the nose (Figure 5A). We observed habenular responses upon both odor delivery and dorsal forebrain micro-electrode stimulation (Figures 5B and 5C). We tested whether the habenula has distinct populations of neurons with different preferences for dorsal forebrain and olfactory inputs. Interestingly, a majority of the habenular neurons that are strongly activated by the micro-stimulation of the dorsal forebrain showed weak or no odor responses (Figure 5E), supporting the idea that habenula is composed of distinct zones with sensory or limbic inputs. Moreover, we observed that functional clusters of habenula based on ongoing neural activity also remain stable during sequential odor and forebrain stimulation (Figure S5), supporting the idea that odors and forebrain inputs activate relatively distinct functional clusters of the habenula.

Next, we asked whether chemosensory and limbic inputs to habenula can influence each other when they are delivered simultaneously (Figure 5D). We first visualized the influence of dorsal forebrain stimulation on the habenular odor responses by plotting the odor responses of habenular neurons against the change of their odor responses in the presence of forebrain stimulation (Figure 5F). In fact, 18.3% of odor-responding habenular neurons showed a significant change in their odor responses upon forebrain stimulation (Figure 5F, black). The majority of these significantly modulated odor responses were weakly odor-responding habenular neurons, whose responses were potentiated by forebrain stimulation. Next, we asked

(H) Responses of habenular neurons upon Dm micro-stimulation clustered by k-means clustering. Forebrain micro-stimulations are marked in red. Warm colors represent higher neural activity.
(I) The ratio of habenular neuron pairs remaining in the same functional clusters (high cluster fidelity) is significantly higher than chance levels during ongoing activity and Dm micro-stimulation. ***$p < 0.001$, Wilcoxon signed-rank test.
(J) Two-photon calcium signals upon electrical micro-stimulation of forebrain region Dl in *Tg(eval3:GCaMP5)* juvenile zebrafish brain explant. Cyan triangle represents electrode location. Habenula and Dl are delineated with dashed lines.
(K) Reconstruction of habenular responses upon Dl micro-stimulation.
(L) Histogram representing the responses of habenular neurons upon Dl micro-stimulation (575 ± 92 neurons per fish, in n = 6 fish). Pie chart represents the ratio of habenular neurons that are activated 2 SDs higher than baseline levels upon Dl micro-stimulation.
(M) Relation between pairwise correlation of habenular neuron responses upon Dl micro-stimulation and the distance between each neuron pair. Gray line represents shuffled spatial distribution.
(N) Reconstruction of habenular neurons clustered with k-means functional clustering of their ongoing activity in juvenile zebrafish brain explant. Colors represent habenular clusters with similar ongoing activity. L, left; R, right hemisphere.
(O) Ongoing activity of the habenular neurons corresponding to clusters in (N).
(P) Reconstruction of habenular neurons clustered during Dl micro-stimulation using k-means clustering. Colors represent habenular clusters with similar responses to Dl micro-stimulation. L, left; R, right hemisphere.
(Q) Responses of habenular neurons upon Dl micro-stimulation clustered by k-means clustering. Forebrain micro-stimulations are marked in red.
(R) The ratio of habenular neuron pairs remaining in the same functional clusters (high cluster fidelity) is significantly higher than chance levels during ongoing activity and Dl micro-stimulation. ***$p < 0.001$, Wilcoxon signed-rank test.
See also Figure S4.

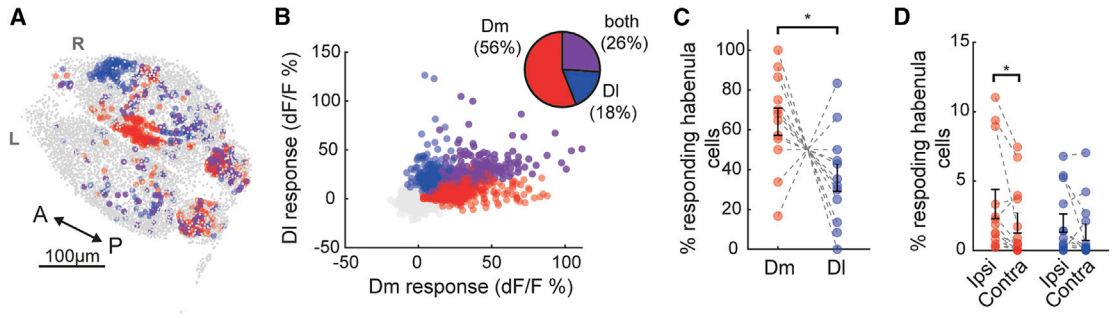

Figure 4. Activating Dm and Dl recruits partially overlapping but different sets of habenular neurons

(A) Representative example of three-dimensional forebrain reconstruction in *Tg(eval3:GCaMP6-nuclear)* juvenile zebrafish brain explant. Neurons are color coded based on their response to Dm (red), Dl (blue), or both (magenta) stimulations, above 2 SDs higher than baseline levels. Non-responding neurons are marked in gray. Scale bar represents 100 μm; L, left; R, right; A, anterior; P, posterior.

(B) Responses of 8,703 individual habenular neurons to Dm (red) and Dl (blue) stimulation or both (magenta) in 12 experiments. Pie chart represents the ratio of habenular neurons responding at least one stimulation, 2 SDs above baseline levels.

(C) Fraction of responding habenular neurons (above 2 SDs) activated by Dm (red) and Dl (blue) stimulations in the same brain explant, n = 12. Note that significantly lager fraction of habenular neurons responds to Dm stimulation compared to Dl stimulation (*$p < 0.05$, tailed Wilcoxon signed-rank test).

(D) Ratio of neurons in each habenular hemisphere activated by the stimulation of Dm (red) and Dl (blue) regions that are located in ipsilateral versus contralateral hemispheres. While Dm stimulation recruits a significantly larger fraction of neurons in ipsilateral hemisphere, Dl stimulation recruits a similar fraction of neurons in both habenular hemispheres (*$p < 0.05$, tailed Wilcoxon signed-rank test).

See also Figure S4.

whether odor stimuli can modulate the responses of habenular neurons to forebrain stimulation. We observed that odor delivery significantly modulates forebrain-driven responses in 21.7% of habenular neurons (Figure 5G, black), with a broad preference for inhibition of forebrain responses in the habenula, during odor stimulation (negative values in y axis, Figure 5G). These results indicate that the habenula integrates chemosensory and limbic information, and that these two different types of inputs can modulate each other, with a prominent suppression of limbic inputs during odor stimulation.

Chemosensory stimulation modulates the ongoing activity of habenular neurons that are functionally coupled with limbic forebrain regions

Our results combining odor delivery with forebrain micro-stimulation in zebrafish brain explant showed that chemosensory stimulation can modulate the activity of habenular neurons that receive forebrain inputs. We asked whether such odor-induced modulation of limbic forebrain-driven habenular neurons is present *in vivo*. To test this, we first identified habenular neurons that are strongly (top 5%) inhibited (in blue) or excited (in red) by a range of attractive and aversive odors (Figures 6A and 6B) and calculated the average ongoing activity of these neurons (Figure 6C). Next, we identified the top 5% of forebrain neurons (Figure 6D), which are strongly correlated with the ongoing activity of habenular neurons that are either strongly inhibited or excited by odors. Finally, we determined how these forebrain neurons with strong correlations to odor-modulated habenular neurons are distributed into anatomically identified distinct forebrain regions, as described in Figures 2E and 2F. Our results revealed that zebrafish homolog of hippocampus Dl contains the largest number of neurons that are highly correlated with odor-modulated (excited and inhabited) habenular neurons (Figure 6E). In fact, Dl is the only forebrain region that contains neurons correlated with odor-modulated habenular neurons (Figure 6E, blue and red labels) significantly more than the shuffled chance levels dictated by the size of individual regions (Figure 6E, dashed line). We did not observe any difference in the effect of aversive or attractive odors (Figures S6A and S6B). Our observations were also robust at different thresholds for selecting forebrain neurons strongly correlated with odor-modulated habenular neurons (Figures S6C and S6D).

Our results demonstrate the presence of strong chemosensory modulation (excitation/inhibition) of limbic-driven habenular activity. Yet it is not clear if such chemosensory modulation happens at the level of habenular neurons or also at the level of limbic forebrain regions of zebrafish. To investigate the distribution of chemosensory modulation of dorsal forebrain neurons, we determined odor responses across the forebrain. Our results showed that Dl is the only forebrain region with odor-inhibited neurons significantly above chance levels (Figure 6F, top). As expected, OB and olfactory cortex (Dp)[71] have the largest fraction of odor excited neurons that are also significantly above the chance levels, in addition to dorsal zone of dorsal telencephalon (Dd) (Figure 6F, bottom). We observed no significant differences in the distribution of attractive or aversive odor responses (Figures S6E and S6F). The locations of forebrain regions that are strongly (top 5%) inhibited (blue) or excited (red) by odors are highlighted in Figure 6G.

Next, we asked how much of this odor-induced excitation and inhibition across the forebrain can explain the odor modulation of habenular activity. To do this, we first identified neurons of specific forebrain regions that are strongly correlated (top 5%) with the activity of odor-inhibited or odor-excited habenular neurons. We then asked what percent of these habenula-correlated forebrain neurons are modulated by odors. We observed that only a very small fraction (less than 5%–10%) of forebrain neurons that are driving odor-modulated habenular neurons are inhibited (blue) or excited (red) by odors (Figures 6H and 6I). This finding suggests that odors can separately modulate the limbic forebrain and habenular neurons with limited functional connections,

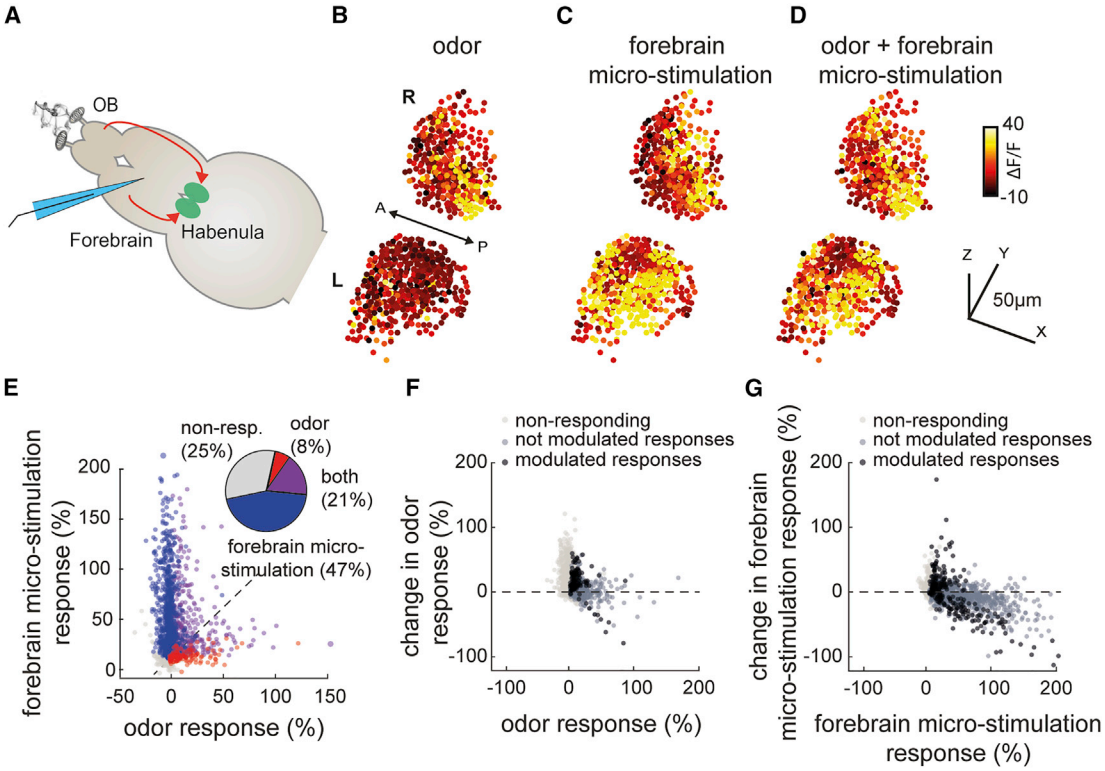

Figure 5. Habenular neurons integrate inputs from limbic dorsal forebrain regions and olfactory system in a non-linear manner

(A) Schematic representation of nose-attached brain-explant preparation in *Tg(elavl3:GCaMP6s)* juvenile zebrafish, allowing simultaneous micro-stimulation of dorsal forebrain and odor stimulation of the nose. Habenula is marked in green; stimulation electrode is marked in cyan. Red arrows represent olfactory and dorsal forebrain inputs.

(B) Three-dimensional reconstruction of habenular responses to odor stimulation averaged over 6 trials. Warm colors indicate stronger neural responses. L, left; R, right hemisphere.

(C) Three-dimensional reconstruction of habenular responses to dorsal forebrain micro-stimulation averaged over 6 trials.

(D) Three-dimensional reconstruction of habenular responses to simultaneous odor stimulation and dorsal forebrain micro-stimulation averaged over 6 trials.

(E) Responses of individual habenular neurons to odor stimulation and dorsal forebrain micro-stimulation from 2,550 neurons measured in n = 5 fish. Pie chart represents the ratio of habenular neurons responding 2 SDs above baseline levels to only odors (red), only micro-stimulation (blue), and both (magenta).

(F) Change of odor responses in habenular neurons upon dorsal forebrain stimulation. Dark gray marks habenular neurons responding to odor stimulation. Black marks habenular neurons responding to odor stimulation and that are significantly ($p < 0.05$, Wilcoxon signed-rank test) modulated by forebrain micro-stimulation.

(G) Change of habenular neuron responses to dorsal forebrain activation upon odor stimulation. Dark gray marks habenular neurons responding to dorsal forebrain micro-stimulation. Black marks habenular neurons responding to dorsal forebrain micro-stimulation and that are significantly ($p < 0.05$, Wilcoxon signed-rank test) modulated by the presentation of odors.

See also Figure S5.

and that the odor modulation of habenular activity is recruited on top of the odor responses that we observed in the forebrain. Altogether, our results revealed that odors inhibit the activity of the ancestral limbic forebrain circuits in zebrafish. We also showed that odor-induced modulation of habenular activity cannot solely be explained by the odor responses of forebrain neurons. These findings suggest that odor stimulation not only alters the dynamics of the forebrain circuitry but also changes the way habenula integrates its forebrain inputs, and further modulates the state of ongoing habenular activity.

DISCUSSION

In this study, we revealed the forebrain circuitry underlying ongoing habenular activity and showed that this inter-connected network can generate structured ongoing activity with strong synchrony and anti-synchrony that is stable over time. Our results further showed that chemosensory stimuli can modulate brain activity not only by activating the olfactory pathway, but also by suppressing the ongoing activity of habenular networks and its input regions in the forebrain that are ancestral to mammalian limbic system. Interestingly, our micro-stimulation experiments also revealed that the specific communication between habenula and its forebrain inputs is dampened in the presence of odor stimulation. Disruption of ongoing (or resting state) brain activity with sensory stimuli has also been observed in human subjects,[2,4,5] suggesting a high level of evolutionary conservation (or convergent evolution) of vertebrate brain dynamics and the way they interact with the sensory world. Such interactions could serve multiple purposes. First, disruption of ongoing

CellPress
OPEN ACCESS

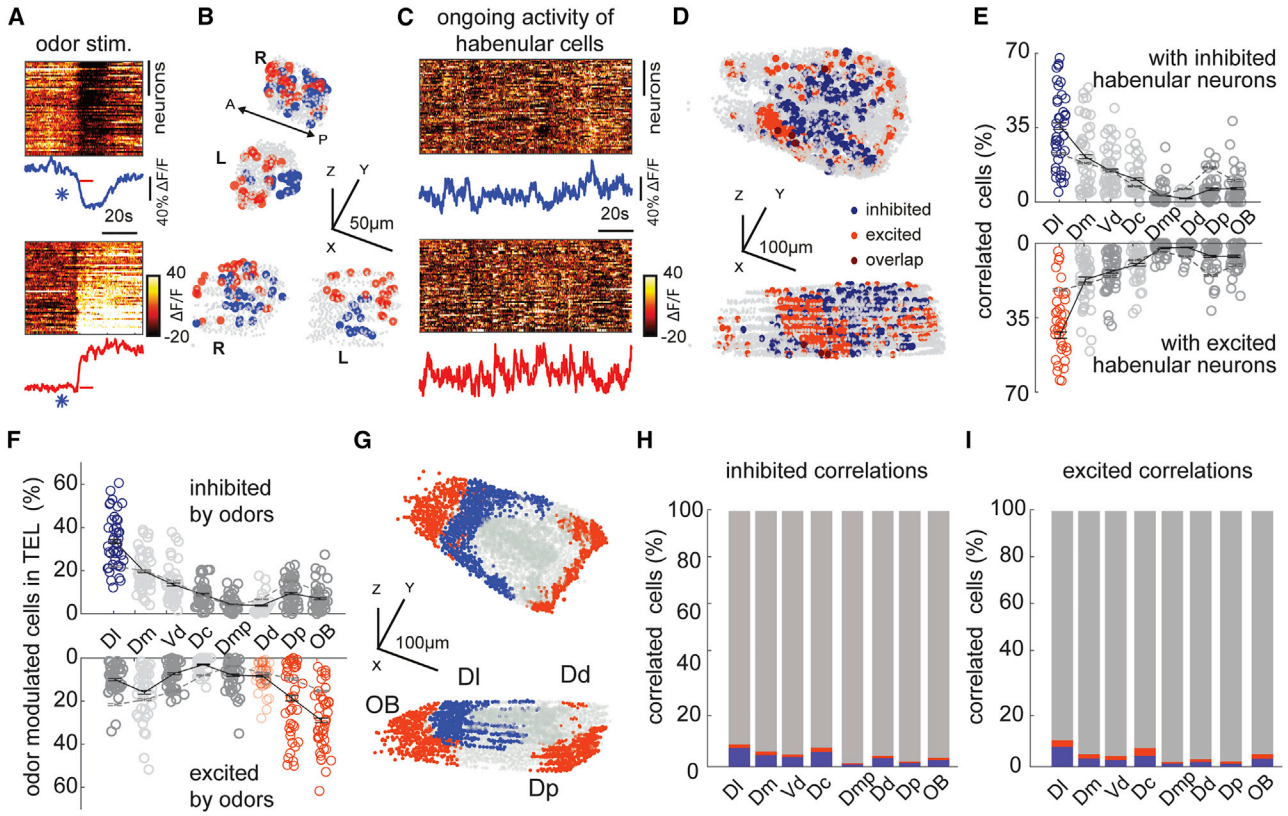

Figure 6. Odor-modulated habenular neurons are functionally connected with limbic dorsal forebrain regions during ongoing activity

(A) Representative example of habenular responses to the odor stimulation recorded by two-photon calcium imaging in *Tg(eval3:GCaMP6s)* zebrafish line. Distinct populations of habenular neurons are inhibited (top) and excited (bottom) upon odor stimulation. Dark colors represent inhibition (top 5% most inhibited neurons). Warm colors represent excitation (top 5% most excited neurons). Individual traces represent average inhibition (blue) and excitation (red) of habenular neurons. Asterisk indicates opening of odor valve; red bar indicates odor presentation.

(B) Representative example of three-dimensional reconstruction of top 5% odor inhibited (blue) and excited (red) habenular neurons from an individual fish. 916 ± 39 (mean ± SEM) habenular neurons were imaged in n = 10 fish.

(C) Ongoing neural activity of odor-inhibited (top) and odor-excited (bottom) habenular neurons in (B). Lines represent the average ongoing activity of odor-inhibited (blue) and odor-excited (red) habenular neurons.

(D) Representative example of three-dimensional reconstruction of top 5% forebrain neurons that are correlated with the ongoing activity of odor-inhibited (blue) and odor-excited (red) habenular neurons. 5,799 ± 165 (mean ± SEM) forebrain neurons were imaged in n = 10 fish.

(E) Anatomical distribution of forebrain neurons with strong correlations (top 5%) to ongoing activity of habenular neurons that are inhibited (top) and excited (bottom) by odors. Red and blue colored circles highlight those forebrain regions that exhibit significantly higher synchrony to habenular neurons than the shuffled chance levels dictated by the size of individual regions. $p < 0.01$, Wilcoxon signed-rank test. Black lines represent mean ± SEM (n = 10 fish). Dl, dorsolateral telencephalon; Dd, dorsal nucleus of the dorsal telencephalon; Dm, dorsomedial telencephalon; Dp, posterior zone of the dorsal telencephalon; Vd, dorsal nucleus of the ventral telencephalon; OB, olfactory bulb; Dmp, posterior nucleus of dorsomedial telencephalon; Dc, central zone of the dorsal telencephalon.

(F) Anatomical distribution of forebrain neurons that are most (top 5%) inhibited (top) and most excited (bottom) by odors. Colored circles highlight those forebrain regions that exhibit significantly higher number of odor-inhibited (blue) and odor-excited (red) neurons than the shuffled chance levels dictated by the size of individual regions. $p < 0.01$, Wilcoxon signed-rank test. Black lines represent mean ± SEM (n = 10 fish). Dl, dorsolateral telencephalon; Dd, dorsal nucleus of the dorsal telencephalon; Dm, dorsomedial telencephalon; Dp, posterior zone of the dorsal telencephalon; Vd, dorsal nucleus of the ventral telencephalon; OB, olfactory bulb; Dmp, posterior nucleus of dorsomedial telencephalon; Dc, central zone of the dorsal telencephalon.

(G) Three-dimensional representation of forebrain regions that show significantly higher number of odor-inhibited (blue) and odor-excited (red) neurons than the shuffled chance levels dictated by the size of individual regions as in (F). Dl, dorsolateral telencephalon; Dd, dorsal nucleus of the dorsal telencephalon; Dp, posterior zone of the dorsal telencephalon; OB, olfactory bulb.

(H) Overlap of odor-responding (blue, inhibited; red, excited) neurons in each forebrain region and forebrain neurons that drive odor-inhibited habenular neurons.

(I) Overlap of odor-responding (blue, inhibited; red, excited) neurons in each forebrain region and forebrain neurons that drive odor-excited habenular neurons.

See also Figure S6.

or resting brain state by a salient sensory stimulus can facilitate state transitions, when an animal needs to quickly attend, adapt, and respond to salient environmental changes. In fact, such a role of the habenula in behavioral flexibility and adapting to new conditions has been demonstrated in both zebrafish[6,36,37,41,42,45] and mammals.[1,82] Second, dampening of ongoing habenular and forebrain activity might increase the sensitivity of these networks to incoming sensory information by reducing background noise levels. This would, in turn, increase the robustness of sensory representations of incoming

stimuli following the first encounter,[83] as is often the case with olfactory stimuli that are received by repeated exposure to odor plumes.[84,85] Finally, resetting the ongoing activity of limbic forebrain networks might be an important mechanism allowing animals to make new associations when conditions are altered, as has been shown during reversal learning.[1,44,46,82] Discovering how the ongoing activity of these networks adapts during behavioral plasticity and learning will require well-established behavioral assays and simultaneous imaging of forebrain and habenular activity in juvenile zebrafish that can perform cognitively demanding learning tasks.[44,59–62] Moreover, given the multi-sensory responses of habenular circuits,[29] it will also be interesting to test whether such interactions between sensory stimuli and ongoing brain activity generalize to other sensory modalities (e.g., vision, auditory) in future studies.

Anatomical projections from the OB,[17,70] entopeduncular nucleus,[20,27,32,34,86,87] and lateral hypothalamus[20,25,64] to habenula have been shown by several past studies. In addition to these anatomically confirmed regions, our results showed that Dl and Dm, zebrafish homologs of mammalian hippocampus and amygdala, are the main dorsal forebrain regions that are strongly correlated with ongoing habenular activity. It is yet to be discovered whether each distinct habenular sub-circuit encodes information from different forebrain regions. Our results showed a small but significant preference for the functional clusters located in dorsal regions of the habenula to be correlated to Dm and OB, and ventral functional clusters as well as genetically tagged vHb[36] neurons to be significantly more correlated to Dl activity, and less with Dm and OB. Moreover, we also confirmed our correlation-based functional connectivity measures by further micro-stimulation of Dl and Dm that activate a partially overlapping but distinct population of habenular neurons. We also observed that stimulating Dm recruits a larger number of neurons when compared to Dl, and preferentially in the ipsilateral habenular hemisphere. These findings suggest that the functional connections relaying information from Dm or Dl to the habenula might take partially overlapping but distinct pathways. To our knowledge, no direct anatomical projections from Dl or Dm were reported to innervate habenula in zebrafish. Hence, functional inputs originating from Dm or Dl to habenula are most likely to be polysynaptic, rather than direct connections. For example, Dm neurons were shown to innervate ventral entopeduncular nucleus[68] and hypothalamus,[68] both of which were shown to project and strongly regulate habenular activity in zebrafish and mammals.[20,25,33,34,64,65,79,81] Dl neurons are a larger group of neurons that are likely functionally heterogenous due to the large size of the Dl region. All studies of Dl in teleost fish highlight a homology of this structure with hippocampal-entorhinal circuitry related to episodic memory and spatial navigation.[75–77,80,88] In fact, similar to our findings in zebrafish, functional coupling between hippocampal circuitry and habenula has been shown also in rodents.[89–91] All these results suggest that hippocampal circuitry can communicate with the habenula, but likely through indirect and polysynaptic connections, such as through ventral entopeduncular nucleus or hypothalamus. Future studies will be needed to map distinct polysynaptic pathways linking hippocampal circuitry to habenula.

It is also important to note that any functional connectivity measure based on correlation of slow calcium signals has limitations, and it is difficult to predict what connects to what in the brain, purely by synchronous calcium activity. For example, slow timescale of calcium signals might limit the interpretation of any correlation-based functional connectivity analysis as we used here. To mitigate this, we showed that our critical findings in ongoing habenular activity and forebrain-habenula interactions can be reproduced using temporally deconvolving calcium signals.[92] Future studies using genetically encoded voltage sensors[93] and fast volumetric imaging will open new avenues for functional connectivity analysis with better datasets. We also supported our functional connectivity measures by micro-electrode stimulations of distinct forebrain regions (Dm and Dl), while imaging habenular calcium signals. It is difficult to completely rule out that micro-stimulation electrodes targeting Dm or Dl might directly activate habenula or activate descending axons in the forebrain. To rule out these possibilities, we stimulated a control forebrain region that is spatially even closer to habenula (Dp/Dmp) (Figures S4J–S4O). These control experiments did not elicit significant habenular activity, demonstrating the strength and specificity of our Dm and Dl micro-stimulation approach. Finally, we also showed that activating forebrain in the presence of synaptic transmission blockers abolished habenular responses, which rules out the possibility of direct electrical activation. Yet further work is needed to functionally dissect zebrafish forebrain and its connections to the habenula. For example, extensive anatomical and molecular reconstructions of forebrain neurons, by using newly generated electron and light microscopy imaging datasets from zebrafish brains,[67,94] will be crucial to better understand zebrafish forebrain anatomy and relate it to mammals. Similarly, optogenetic stimulation of specific forebrain regions combined with intracellular recordings will shed more light onto direct or polysynaptic connections between distinct forebrain regions and habenula.

As small vertebrates, zebrafish exhibit general principles of vertebrate forebrain architecture. Most studies of zebrafish forebrain circuitry have investigated adult zebrafish with sophisticated behaviors and large brains that are challenging to access using optical imaging methods and require surgery.[79,95] The forebrain, especially the dorsal telencephalon, of transparent 5- to 10-day-old zebrafish larvae is not yet fully developed.[29,81,96] Hence, using 3- to 4-week-old juvenile zebrafish provides an alternative approach to study a relatively developed forebrain network[29,81,96] that is still optically accessible for imaging the entire forebrain, including habenula, as we demonstrated in this study. This approach allowed us to identify functionally distinct populations of forebrain neurons, which also overlapped with distinct forebrain regions that we could identify based on anatomical landmarks. Despite its limitations, such as slow kinetics and sensitivity, our calcium imaging results allowed us to relate some of these functionally defined zones in juvenile zebrafish forebrain with adult zebrafish, other teleosts, and even mammalian forebrain structures. Future studies of molecular profiling, anatomical reconstructions, and neural connectivity of forebrain neurons will be important to further support our calcium imaging-based functional clustering and connectivity measures. Given the ability of juvenile zebrafish to perform cognitively demanding behaviors such as social interactions[62,63] and learning,[44,59–61] while allowing non-invasive functional imaging, we hope that combinations of these approaches will shed

further light onto the function and connectivity of forebrain networks during these behaviors.

Altogether, our results highlight the activity and connectivity of forebrain networks underlying ongoing habenular activity and reveal how habenula integrates olfactory and limbic information. Our findings further support the idea that the habenula serves as a main hub,[22,43] which can integrate sensory and non-sensory information from diverse forebrain regions and relays this integrated information to its downstream targets regulating animal behavior.[20–26,28,34] Given the important role of habenula in adaptive behaviors and mood disorders,[47,48] our results suggest that sensory experience might provide a non-invasive pathway to modulate habenular activity, perhaps also in humans. Future studies with high-throughput and high-resolution brain imaging methods in mammals may answer whether sensory information can perturb the dynamics of ongoing activity of mammalian habenula.

STAR★METHODS

Detailed methods are provided in the online version of this paper and include the following:

- KEY RESOURCES TABLE
- RESOURCE AVAILABILITY
  - Lead contact
  - Materials availability
  - Data and code availability
- EXPERIMENTAL MODEL AND SUBJECT DETAILS
  - Zebrafish maintenance and strains
  - Ethical guidelines statement
- METHOD DETAILS
  - Two-photon calcium imaging
  - Odor preparation
  - Odor delivery
  - Micro-electrode stimulation
  - Dissection of juvenile zebrafish brain explant
- QUANTIFICATION AND STATISTICAL ANALYSIS
  - Statistics

SUPPLEMENTAL INFORMATION

Supplemental information can be found online at https://doi.org/10.1016/j.cub.2021.08.021.

ACKNOWLEDGMENTS

We thank M. Ahrens (HHMI, Janelia Farm, USA), K. Kawakami (NIG, Japan), and H. Okamoto (RIKEN-CBS, Japan) for transgenic lines; S. Eggen, M. Andresen, V. Nguyen, and our fish facility support team for technical assistance; the Yaksi lab members for stimulating discussions; and Steffen Kandler and Nathalie Jurisch-Yaksi for their feedback on the manuscript. This work was funded by ERC starting grant 335561 (E.Y.), NFR FRIPRO research grants 239973 and 314212 (E.Y.), and Boehringer Ingelheim Fonds (S.K.J.). Work in the Yaksi lab is funded by the Kavli Institute for Systems Neuroscience at NTNU.

AUTHOR CONTRIBUTIONS

Conceptualization, E.M.B., A.M.O., S.K.J., and E.Y.; Methodology and Analysis, E.M.B., A.M.O., S.K.J., B.S., A.K.M., K.T.P.C., and E.Y.; Investigation, all authors; Writing, E.M.B., A.M.O., and E.Y.; Review & Editing, all authors; Funding Acquisition and Supervision, E.Y.

DECLARATION OF INTERESTS

The authors declare no competing interests.

INCLUSION AND DIVERSITY

We worked to ensure sex balance in the selection of non-human subjects. One or more of the authors of this paper self-identifies as an underrepresented ethnic minority in science. One or more of the authors of this paper self-identifies as a member of the LGBTQ+ community.

Received: March 17, 2021
Revised: July 13, 2021
Accepted: August 5, 2021
Published: August 19, 2021

REFERENCES

1. Baker, P.M., Oh, S.E., Kidder, K.S., and Mizumori, S.J. (2015). Ongoing behavioral state information signaled in the lateral habenula guides choice flexibility in freely moving rats. Front. Behav. Neurosci. *9*, 295.
2. Raichle, M.E., MacLeod, A.M., Snyder, A.Z., Powers, W.J., Gusnard, D.A., and Shulman, G.L. (2001). A default mode of brain function. Proc. Natl. Acad. Sci. USA *98*, 676–682.
3. Raichle, M.E. (2015). The brain's default mode network. Annu. Rev. Neurosci. *38*, 433–447.
4. Greicius, M.D., and Menon, V. (2004). Default-mode activity during a passive sensory task: uncoupled from deactivation but impacting activation. J. Cogn. Neurosci. *16*, 1484–1492.
5. Shulman, G.L., Fiez, J.A., Corbetta, M., Buckner, R.L., Miezin, F.M., Raichle, M.E., and Petersen, S.E. (1997). Common blood flow changes across visual tasks: II. Decreases in cerebral cortex. J. Cogn. Neurosci. *9*, 648–663.
6. Andalman, A.S., Burns, V.M., Lovett-Barron, M., Broxton, M., Poole, B., Yang, S.J., Grosenick, L., Lerner, T.N., Chen, R., Benster, T., et al. (2019). Neuronal dynamics regulating brain and behavioral state transitions. Cell *177*, 970–985.e20.
7. Shimaoka, D., Steinmetz, N.A., Harris, K.D., and Carandini, M. (2019). The impact of bilateral ongoing activity on evoked responses in mouse cortex. eLife *8*, e43533.
8. Stringer, C., Pachitariu, M., Steinmetz, N., Reddy, C.B., Carandini, M., and Harris, K.D. (2019). Spontaneous behaviors drive multidimensional, brain-wide activity. Science *364*, 255.
9. Arieli, A., Sterkin, A., Grinvald, A., and Aertsen, A. (1996). Dynamics of ongoing activity: explanation of the large variability in evoked cortical responses. Science *273*, 1868–1871.
10. Romano, S.A., Pietri, T., Pérez-Schuster, V., Jouary, A., Haudrechy, M., and Sumbre, G. (2015). Spontaneous neuronal network dynamics reveal circuit's functional adaptations for behavior. Neuron *85*, 1070–1085.
11. Tsitoura, C., Malinowski, S.T., Mohrhardt, J., Degen, R., DiBenedictis, B.T., Gao, Y., Watznauer, K., Gerhold, K., Nagel, M., Weber, M., et al. (2020). Synchronous infra-slow oscillations organize ensembles of accessory olfactory bulb projection neurons into distinct microcircuits. J. Neurosci. *40*, 4203–4218.
12. Galán, R.F., Weidert, M., Menzel, R., Herz, A.V.M., and Galizia, C.G. (2006). Sensory memory for odors is encoded in spontaneous correlated activity between olfactory glomeruli. Neural Comput. *18*, 10–25.
13. Luo, Y.J., Li, Y.D., Wang, L., Yang, S.R., Yuan, X.S., Wang, J., Cherasse, Y., Lazarus, M., Chen, J.F., Qu, W.M., and Huang, Z.L. (2018). Nucleus accumbens controls wakefulness by a subpopulation of neurons expressing dopamine D_1 receptors. Nat. Commun. *9*, 1576.

14. Hahn, T.T.G., McFarland, J.M., Berberich, S., Sakmann, B., and Mehta, M.R. (2012). Spontaneous persistent activity in entorhinal cortex modulates cortico-hippocampal interaction in vivo. Nat. Neurosci. *15*, 1531–1538.

15. Koyama, S., Kanemitsu, Y., and Weight, F.F. (2005). Spontaneous activity and properties of two types of principal neurons from the ventral tegmental area of rat. J. Neurophysiol. *93*, 3282–3293.

16. Weis, C.N., Huggins, A.A., Bennett, K.P., Parisi, E.A., and Larson, C.L. (2019). High-resolution resting-state functional connectivity of the extended amygdala. Brain Connect. *9*, 627–637.

17. Miyasaka, N., Morimoto, K., Tsubokawa, T., Higashijima, S., Okamoto, H., and Yoshihara, Y. (2009). From the olfactory bulb to higher brain centers: genetic visualization of secondary olfactory pathways in zebrafish. J. Neurosci. *29*, 4756–4767.

18. Cheng, R.K., Krishnan, S., Lin, Q., Kibat, C., and Jesuthasan, S. (2017). Characterization of a thalamic nucleus mediating habenula responses to changes in ambient illumination. BMC Biol. *15*, 104.

19. Zhang, B.B., Yao, Y.Y., Zhang, H.F., Kawakami, K., and Du, J.L. (2017). Left habenula mediates light-preference behavior in zebrafish via an asymmetrical visual pathway. Neuron *93*, 914–928.e4.

20. Turner, K.J., Hawkins, T.A., Yáñez, J., Anadón, R., Wilson, S.W., and Folgueira, M. (2016). Afferent connectivity of the zebrafish habenulae. Front. Neural Circuits *10*, 30.

21. Warden, M.R., Selimbeyoglu, A., Mirzabekov, J.J., Lo, M., Thompson, K.R., Kim, S.Y., Adhikari, A., Tye, K.M., Frank, L.M., and Deisseroth, K. (2012). A prefrontal cortex-brainstem neuronal projection that controls response to behavioural challenge. Nature *492*, 428–432.

22. Okamoto, H., Agetsuma, M., and Aizawa, H. (2012). Genetic dissection of the zebrafish habenula, a possible switching board for selection of behavioral strategy to cope with fear and anxiety. Dev. Neurobiol. *72*, 386–394.

23. Matsumoto, M., and Hikosaka, O. (2007). Lateral habenula as a source of negative reward signals in dopamine neurons. Nature *447*, 1111–1115.

24. Meye, F.J., Soiza-Reilly, M., Smit, T., Diana, M.A., Schwarz, M.K., and Mameli, M. (2016). Shifted pallidal co-release of GABA and glutamate in habenula drives cocaine withdrawal and relapse. Nat. Neurosci. *19*, 1019–1024.

25. Lazaridis, I., Tzortzi, O., Weglage, M., Märtin, A., Xuan, Y., Parent, M., Johansson, Y., Fuzik, J., Fürth, D., Fenno, L.E., et al. (2019). A hypothalamus-habenula circuit controls aversion. Mol. Psychiatry *24*, 1351–1368.

26. Stamatakis, A.M., Jennings, J.H., Ung, R.L., Blair, G.A., Weinberg, R.J., Neve, R.L., Boyce, F., Mattis, J., Ramakrishnan, C., Deisseroth, K., and Stuber, G.D. (2013). A unique population of ventral tegmental area neurons inhibits the lateral habenula to promote reward. Neuron *80*, 1039–1053.

27. Hong, S., Jhou, T.C., Smith, M., Saleem, K.S., and Hikosaka, O. (2011). Negative reward signals from the lateral habenula to dopamine neurons are mediated by rostromedial tegmental nucleus in primates. J. Neurosci. *31*, 11457–11471.

28. Herkenham, M., and Nauta, W.J. (1977). Afferent connections of the habenular nuclei in the rat. A horseradish peroxidase study, with a note on the fiber-of-passage problem. J. Comp. Neurol. *173*, 123–146.

29. Fore, S., Acuña-Hinrichsen, F., Mutlu, K.A., Bartoszek, E.M., Serneels, B., Faturos, N.G., Chau, K.T.P., Cosacak, M.I., Verdugo, C.D., Palumbo, F., et al. (2020). Functional properties of habenular neurons are determined by developmental stage and sequential neurogenesis. Sci. Adv. *6*, eaaz3173.

30. Jetti, S.K., Vendrell-Llopis, N., and Yaksi, E. (2014). Spontaneous activity governs olfactory representations in spatially organized habenular microcircuits. Curr. Biol. *24*, 434–439.

31. Yang, Y., Cui, Y., Sang, K., Dong, Y., Ni, Z., Ma, S., and Hu, H. (2018). Ketamine blocks bursting in the lateral habenula to rapidly relieve depression. Nature *554*, 317–322.

32. Stephenson-Jones, M., Floros, O., Robertson, B., and Grillner, S. (2012). Evolutionary conservation of the habenular nuclei and their circuitry controlling the dopamine and 5-hydroxytryptophan (5-HT) systems. Proc. Natl. Acad. Sci. USA *109*, E164–E173.

33. Bromberg-Martin, E.S., Matsumoto, M., Hong, S., and Hikosaka, O. (2010). A pallidus-habenula-dopamine pathway signals inferred stimulus values. J. Neurophysiol. *104*, 1068–1076.

34. Hendricks, M., and Jesuthasan, S. (2007). Asymmetric innervation of the habenula in zebrafish. J. Comp. Neurol. *502*, 611–619.

35. Hong, E., Santhakumar, K., Akitake, C.A., Ahn, S.J., Thisse, C., Thisse, B., Wyart, C., Mangin, J.M., and Halpern, M.E. (2013). Cholinergic left-right asymmetry in the habenulo-interpeduncular pathway. Proc. Natl. Acad. Sci. USA *110*, 21171–21176.

36. Amo, R., Fredes, F., Kinoshita, M., Aoki, R., Aizawa, H., Agetsuma, M., Aoki, T., Shiraki, T., Kakinuma, H., Matsuda, M., et al. (2014). The habenulo-raphe serotonergic circuit encodes an aversive expectation value essential for adaptive active avoidance of danger. Neuron *84*, 1034–1048.

37. Duboué, E.R., Hong, E., Eldred, K.C., and Halpern, M.E. (2017). Left habenular activity attenuates fear responses in larval zebrafish. Curr. Biol. *27*, 2154–2162.e3.

38. Lin, Q., and Jesuthasan, S. (2017). Masking of a circadian behavior in larval zebrafish involves the thalamo-habenula pathway. Sci. Rep. *7*, 4104.

39. Baker, P.M., Raynor, S.A., Francis, N.T., and Mizumori, S.J. (2017). Lateral habenula integration of proactive and retroactive information mediates behavioral flexibility. Neuroscience *345*, 89–98.

40. Kawai, T., Yamada, H., Sato, N., Takada, M., and Matsumoto, M. (2015). Roles of the lateral habenula and anterior cingulate cortex in negative outcome monitoring and behavioral adjustment in nonhuman primates. Neuron *88*, 792–804.

41. Chou, M.Y., Amo, R., Kinoshita, M., Cherng, B.W., Shimazaki, H., Agetsuma, M., Shiraki, T., Aoki, T., Takahoko, M., Yamazaki, M., et al. (2016). Social conflict resolution regulated by two dorsal habenular subregions in zebrafish. Science *352*, 87–90.

42. Agetsuma, M., Aizawa, H., Aoki, T., Nakayama, R., Takahoko, M., Goto, M., Sassa, T., Amo, R., Shiraki, T., Kawakami, K., et al. (2010). The habenula is crucial for experience-dependent modification of fear responses in zebrafish. Nat. Neurosci. *13*, 1354–1356.

43. Fore, S., Palumbo, F., Pelgrims, R., and Yaksi, E. (2018). Information processing in the vertebrate habenula. Semin. Cell Dev. Biol. *78*, 130–139.

44. Palumbo, F., Serneels, B., Pelgrims, R., and Yaksi, E. (2020). The zebrafish dorsolateral habenula is required for updating learned behaviors. Cell Rep. *32*, 108054.

45. Lee, A., Mathuru, A.S., Teh, C., Kibat, C., Korzh, V., Penney, T.B., and Jesuthasan, S. (2010). The habenula prevents helpless behavior in larval zebrafish. Curr. Biol. *20*, 2211–2216.

46. Cherng, B.W., Islam, T., Torigoe, M., Tsuboi, T., and Okamoto, H. (2020). The dorsal lateral habenula-interpeduncular nucleus pathway is essential for left-right-dependent decision making in zebrafish. Cell Rep. *32*, 108143.

47. Sartorius, A., Kiening, K.L., Kirsch, P., von Gall, C.C., Haberkorn, U., Unterberg, A.W., Henn, F.A., and Meyer-Lindenberg, A. (2010). Remission of major depression under deep brain stimulation of the lateral habenula in a therapy-refractory patient. Biol. Psychiatry *67*, e9–e11.

48. Lawson, R.P., Nord, C.L., Seymour, B., Thomas, D.L., Dayan, P., Pilling, S., and Roiser, J.P. (2017). Disrupted habenula function in major depression. Mol. Psychiatry *22*, 202–208.

49. Aizawa, H., Kobayashi, M., Tanaka, S., Fukai, T., and Okamoto, H. (2012). Molecular characterization of the subnuclei in rat habenula. J. Comp. Neurol. *520*, 4051–4066.

50. deCarvalho, T.N., Subedi, A., Rock, J., Harfe, B.D., Thisse, C., Thisse, B., Halpern, M.E., and Hong, E. (2014). Neurotransmitter map of the asymmetric dorsal habenular nuclei of zebrafish. Genesis *52*, 636–655.

51. Pandey, S., Shekhar, K., Regev, A., and Schier, A.F. (2018). Comprehensive identification and spatial mapping of habenular neuronal types using single-cell RNA-seq. Curr. Biol. *28*, 1052–1065.e7.

52. Amo, R., Aizawa, H., Takahoko, M., Kobayashi, M., Takahashi, R., Aoki, T., and Okamoto, H. (2010). Identification of the zebrafish ventral habenula as a homolog of the mammalian lateral habenula. J. Neurosci. *30*, 1566–1574.

53. Dreosti, E., Vendrell Llopis, N., Carl, M., Yaksi, E., and Wilson, S.W. (2014). Left-right asymmetry is required for the habenulae to respond to both visual and olfactory stimuli. Curr. Biol. *24*, 440–445.

54. Kermen, F., Darnet, L., Wiest, C., Palumbo, F., Bechert, J., Uslu, O., and Yaksi, E. (2020). Stimulus-specific behavioral responses of zebrafish to a large range of odors exhibit individual variability. BMC Biol. *18*, 66.

55. Reiten, I., Uslu, F.E., Fore, S., Pelgrims, R., Ringers, C., Diaz Verdugo, C., Hoffman, M., Lal, P., Kawakami, K., Pekkan, K., et al. (2017). Motile-cilia-mediated flow improves sensitivity and temporal resolution of olfactory computations. Curr. Biol. *27*, 166–174.

56. Diaz Verdugo, C., Myren-Svelstad, S., Aydin, E., Van Hoeymissen, E., Deneubourg, C., Vanderhaeghe, S., Vancraeynest, J., Pelgrims, R., Cosacak, M.I., Muto, A., et al. (2019). Glia-neuron interactions underlie state transitions to generalized seizures. Nat. Commun. *10*, 3830.

57. Vladimirov, N., Mu, Y., Kawashima, T., Bennett, D.V., Yang, C.T., Looger, L.L., Keller, P.J., Freeman, J., and Ahrens, M.B. (2014). Light-sheet functional imaging in fictively behaving zebrafish. Nat. Methods *11*, 883–884.

58. Vendrell-Llopis, N., and Yaksi, E. (2015). Evolutionary conserved brainstem circuits encode category, concentration and mixtures of taste. Sci. Rep. *5*, 17825.

59. Valente, A., Huang, K.H., Portugues, R., and Engert, F. (2012). Ontogeny of classical and operant learning behaviors in zebrafish. Learn. Mem. *19*, 170–177.

60. Yashina, K., Tejero-Cantero, Á., Herz, A., and Baier, H. (2019). Zebrafish exploit visual cues and geometric relationships to form a spatial memory. iScience *19*, 119–134.

61. Palumbo, F., Serneels, B., and Yaksi, E. (2021). Optimized protocol for conditioned place avoidance learning in juvenile zebrafish. STAR Protoc. *2*, 100465.

62. Dreosti, E., Lopes, G., Kampff, A.R., and Wilson, S.W. (2015). Development of social behavior in young zebrafish. Front. Neural Circuits *9*, 39.

63. Hinz, R.C., and de Polavieja, G.G. (2017). Ontogeny of collective behavior reveals a simple attraction rule. Proc. Natl. Acad. Sci. USA *114*, 2295–2300.

64. Lecca, S., Meye, F.J., Trusel, M., Tchenio, A., Harris, J., Schwarz, M.K., Burdakov, D., Georges, F., and Mameli, M. (2017). Aversive stimuli drive hypothalamus-to-habenula excitation to promote escape behavior. eLife *6*, e30697.

65. Shabel, S.J., Proulx, C.D., Trias, A., Murphy, R.T., and Malinow, R. (2012). Input to the lateral habenula from the basal ganglia is excitatory, aversive, and suppressed by serotonin. Neuron *74*, 475–481.

66. Diaz-Verdugo, C., Sun, G.J., Fawcett, C.H., Zhu, P., and Fishman, M.C. (2019). Mating suppresses alarm response in zebrafish. Curr. Biol. *29*, 2541–2546.e3.

67. Kunst, M., Laurell, E., Mokayes, N., Kramer, A., Kubo, F., Fernandes, A.M., Förster, D., Dal Maschio, M., and Baier, H. (2019). A cellular-resolution atlas of the larval zebrafish brain. Neuron *103*, 21–38.e5.

68. Lal, P., Tanabe, H., Suster, M.L., Ailani, D., Kotani, Y., Muto, A., Itoh, M., Iwasaki, M., Wada, H., Yaksi, E., and Kawakami, K. (2018). Identification of a neuronal population in the telencephalon essential for fear conditioning in zebrafish. BMC Biol. *16*, 45.

69. Mueller, T., and Wullimann, M.F. (2009). An evolutionary interpretation of teleostean forebrain anatomy. Brain Behav Evol *74*, 30–42.

70. Miyasaka, N., Arganda-Carreras, I., Wakisaka, N., Masuda, M., Sümbül, U., Seung, H.S., and Yoshihara, Y. (2014). Olfactory projectome in the zebrafish forebrain revealed by genetic single-neuron labelling. Nat. Commun. *5*, 3639.

71. Yaksi, E., von Saint Paul, F., Niessing, J., Bundschuh, S.T., and Friedrich, R.W. (2009). Transformation of odor representations in target areas of the olfactory bulb. Nat. Neurosci. *12*, 474–482.

72. Tabor, K.M., Marquart, G.D., Hurt, C., Smith, T.S., Geoca, A.K., Bhandiwad, A.A., Subedi, A., Sinclair, J.L., Rose, H.M., Polys, N.F., and Burgess, H.A. (2019). Brain-wide cellular resolution imaging of Cre transgenic zebrafish lines for functional circuit-mapping. eLife *8*, e42687.

73. Portavella, M., Torres, B., and Salas, C. (2004). Avoidance response in goldfish: emotional and temporal involvement of medial and lateral telencephalic pallium. J. Neurosci. *24*, 2335–2342.

74. Elliott, S.B., and Maler, L. (2015). Stimulus-induced up states in the dorsal pallium of a weakly electric fish. J. Neurophysiol. *114*, 2071–2076.

75. Ocaña, F.M., Uceda, S., Arias, J.L., Salas, C., and Rodríguez, F. (2017). Dynamics of goldfish subregional hippocampal pallium activity throughout spatial memory formation. Brain Behav Evol *90*, 154–170.

76. Elliott, S.B., Harvey-Girard, E., Giassi, A.C.C., and Maler, L. (2017). Hippocampal-like circuitry in the pallium of an electric fish: possible substrates for recursive pattern separation and completion. J. Comp. Neurol. *525*, 8–46.

77. Rodríguez-Expósito, B., Gómez, A., Martín-Monzón, I., Reiriz, M., Rodríguez, F., and Salas, C. (2017). Goldfish hippocampal pallium is essential to associate temporally discontiguous events. Neurobiol. Learn. Mem. *139*, 128–134.

78. Wullimann, M.F., and Mueller, T. (2004). Teleostean and mammalian forebrains contrasted: evidence from genes to behavior. J. Comp. Neurol. *475*, 143–162.

79. Aoki, T., Kinoshita, M., Aoki, R., Agetsuma, M., Aizawa, H., Yamazaki, M., Takahoko, M., Amo, R., Arata, A., Higashijima, S., et al. (2013). Imaging of neural ensemble for the retrieval of a learned behavioral program. Neuron *78*, 881–894.

80. Fotowat, H., Lee, C., Jun, J.J., and Maler, L. (2019). Neural activity in a hippocampus-like region of the teleost pallium is associated with active sensing and navigation. eLife *8*, e44119.

81. von Trotha, J.W., Vernier, P., and Bally-Cuif, L. (2014). Emotions and motivated behavior converge on an amygdala-like structure in the zebrafish. Eur. J. Neurosci. *40*, 3302–3315.

82. Wang, D., Li, Y., Feng, Q., Guo, Q., Zhou, J., and Luo, M. (2017). Learning shapes the aversion and reward responses of lateral habenula neurons. eLife *6*, e23045.

83. Franco, L.M., and Yaksi, E. (2021). Experience-dependent plasticity modulates ongoing activity in the antennal lobe and enhance odor representations. bioRxiv. https://doi.org/10.1101/2021.04.28.441745.

84. Mafra-Neto, A., and Cardé, R.T. (1994). Fine-scale structure of pheromone plumes modulates upwind orientation of flying moths. Nature *369*, 142–144.

85. Zimmer-Faust, R.K., Finelli, C.M., Pentcheff, N.D., and Wethey, D.S. (1995). Odor plumes and animal navigation in turbulent water flow: a field study. Biol. Bull. *188*, 111–116.

86. Vincent, S.R., McIntosh, C.H., Buchan, A.M., and Brown, J.C. (1985). Central somatostatin systems revealed with monoclonal antibodies. J. Comp. Neurol. *238*, 169–186.

87. Sas, E., and Maler, L. (1991). Somatostatin-like immunoreactivity in the brain of an electric fish (Apteronotus leptorhynchus) identified with monoclonal antibodies. J. Chem. Neuroanat. *4*, 155–186.

88. Vinepinsky, E., Cohen, L., Perchik, S., Ben-Shahar, O., Donchin, O., and Segev, R. (2020). Representation of edges, head direction, and swimming kinematics in the brain of freely-navigating fish. Sci. Rep. *10*, 14762.

89. Aizawa, H., Yanagihara, S., Kobayashi, M., Niisato, K., Takekawa, T., Harukuni, R., McHugh, T.J., Fukai, T., Isomura, Y., and Okamoto, H. (2013). The synchronous activity of lateral habenular neurons is essential for regulating hippocampal theta oscillation. J. Neurosci. *33*, 8909–8921.

90. Goutagny, R., Loureiro, M., Jackson, J., Chaumont, J., Williams, S., Isope, P., Kelche, C., Cassel, J.C., and Lecourtier, L. (2013). Interactions between

the lateral habenula and the hippocampus: implication for spatial memory processes. Neuropsychopharmacology *38*, 2418–2426.

91. Baker, P.M., Rao, Y., Rivera, Z.M.G., Garcia, E.M., and Mizumori, S.J.Y. (2019). Selective functional interaction between the lateral habenula and hippocampus during different tests of response flexibility. Front. Mol. Neurosci. *12*, 245.

92. Yaksi, E., and Friedrich, R.W. (2006). Reconstruction of firing rate changes across neuronal populations by temporally deconvolved Ca2+ imaging. Nat. Methods *3*, 377–383.

93. Abdelfattah, A.S., Kawashima, T., Singh, A., Novak, O., Liu, H., Shuai, Y., Huang, Y.C., Campagnola, L., Seeman, S.C., Yu, J., et al. (2019). Bright and photostable chemigenetic indicators for extended in vivo voltage imaging. Science *365*, 699–704.

94. Hildebrand, D.G.C., Cicconet, M., Torres, R.M.I., Choi, W., Quan, T.M., Moon, J., Wetzel, A.W., Scott Champion, A., Graham, B.J., Randlett, O., et al. (2017). Whole-brain serial-section electron microscopy in larval zebrafish. Nature *545*, 345–349.

95. Huang, K.H., Rupprecht, P., Frank, T., Kawakami, K., Bouwmeester, T., and Friedrich, R.W. (2020). A virtual reality system to analyze neural activity and behavior in adult zebrafish. Nat. Methods *17*, 343–351.

96. Furlan, G., Cuccioli, V., Vuillemin, N., Dirian, L., Muntasell, A.J., Coolen, M., Dray, N., Bedu, S., Houart, C., Beaurepaire, E., et al. (2017). Life-long neurogenic activity of individual neural stem cells and continuous growth establish an outside-in architecture in the teleost pallium. Curr. Biol. *27*, 3288–3301.e3.

97. Kermen, F., Lal, P., Faturos, N.G., and Yaksi, E. (2020). Interhemispheric connections between olfactory bulbs improve odor detection. PLoS Biol. *18*, e3000701.

98. Allen, E.A., Damaraju, E., Plis, S.M., Erhardt, E.B., Eichele, T., and Calhoun, V.D. (2014). Tracking whole-brain connectivity dynamics in the resting state. Cereb. Cortex *24*, 663–676.

STAR★METHODS

KEY RESOURCES TABLE

REAGENT or RESOURCE	SOURCE	IDENTIFIER
Chemicals, peptides, and recombinant proteins		
MS222 (Tricaine methanesulfonate)	Sigma-Aldrich	Cat# E10521
LMP Agarose	Fisher Scientific	Cat# 16520100
PBS	Thermo Fisher Scientific	Cat# BR0014G
NBQX	Tocris (Bio-Techne Ltd)	Cat# No. 0373
d-AP5	Tocris (Bio-Techne Ltd)	Cat# 0106/10
Cadmium chloride	Sigma-Aldrich	Cat# 202908
Alanine	Sigma-Aldrich	Cat# A7627
Phenylalanine	Sigma-Aldrich	Cat# P5482
Methionine	Sigma-Aldrich	Cat# M9625
Histidine	Sigma-Aldrich	Cat# H8125
Cysteine	Sigma-Aldrich	Cat#168149
Arginine	Sigma-Aldrich	Cat# A5006
Glutamic acid	Sigma-Aldrich	Cat# G1251
Taurodeoxycholic acid (TDCA)	Sigma-Aldrich	Cat# T0875
Taurocholic acid (TCA)	Sigma-Aldrich	Cat# T4009
Urea	Sigma-Aldrich	Cat# U5378
Ammonium Chloride	Sigma-Aldrich	Cat# A9434
Zebrafish lines		
Tg(elavl3:GCaMP6s) and	Expresses GCaMP6s panneuronally[57]	ZFIN Cat# ZDB-ALT-141023-1
Tg(elavl3:GCaMP6s-nuclear)	Expresses nuclear GCaMP6s panneuronally[57]	ZFIN Cat# ZDB-ALT-141023-1
Tg(elavl3:GCaMP5)	Expresses GCaMP5s panneuronally[30]	ZFIN Cat# ZDB-FISH-150901-22335
Tg(dao:GAL4VP16; UAS-E1b:NTR-mCherry))	labels vHb neurons in adult and juvenile zebrafish[36]	ZFIN Cat# ZDB-FISH-150901-28994
Tg(narp:GAL4VP16; UAS-E1b:NTR-mCherry)	labels dlHb neurons in adult zebrafish and broadly labels dorsal habenula in 3 weeks old juvenile zebrafish[42]	ZFIN Cat# ZDB-FISH-150901-29851
Software and algorithms		
ImageJ/Fiji	https://fiji.sc/	N/A
Cell detection, Image alignment and processing	[30,55,56]	N/A
Other		
Two-photon microscope	Scientifica	N/A
Two-photon microscope, 7MP	Zeiss	N/A
Sutter Laser puller	Sutter	Model P-200
Bipolar stimulator-1	AMPI	ISO-Flex
Bipolar stimulator-2	Digitimer	DS3

RESOURCE AVAILABILITY

Lead contact

Further information and requests for resources and reagents should be directed to and will be fulfilled by the lead contact, Emre Yaksi (emre.yaksi@ntnu.no).

Materials availability

This study did not generate new unique reagents.

Data and code availability

Calcium imaging data and main associated codes that are used to make figures are available at: https://doi.org/10.5061/dryad.z08kprrd7.

EXPERIMENTAL MODEL AND SUBJECT DETAILS

Zebrafish maintenance and strains

NFSA (Norwegian Food Safety Authority) has approved the animal facility and fish maintenance. Fish were kept in 3,5L tanks in a Tecniplast ZebTec Multilinking System. Constant conditions were maintained: 28.5°C, pH 7.2, 700 μSiemens. 14:10 h light/dark cycle was preserved. Dry food (SDS100 up to 14 dpf and SDS 400 for adult animals, Tecnilab BMI, the Netherlands) was given to fish twice a day, in addition to Artemia nauplii (Grade 0, Platinum Label, Argent Laboratories, Redmond, USA) once a day. From fertilization to 3 dpf (days post fertilization) larvae were kept in a Petri dish with egg water (1.2 g marine salt in 20L RO water, 1:1000 0.1% methylene blue) and between 3 and 5 dpf in artificial fish water (AFW: 1.2 g marine salt in 20L RO water). Juvenile (3 to 4-week-old) zebrafish from were used for the experiments. Animals were used and analyzed irrespective of their gender.

Tg(elavl3:GCaMP5),[30] *Tg(elavl3:GCaMP6s) and Tg(elavl3:GCaMP6s-nuclear)*[57] zebrafish lines were used for two-photon calcium imaging. *Tg(dao:GAL4VP16; UAS-E1b:NTR-mCherry)*[36] line was used to genetically label ventral habenula and (*Tg(narp:GAL4VP16; UAS-E1b:NTR-mCherry)*[42] line was used to genetically label dorsal habenula.

Ethical guidelines statement

All experimental procedures performed on zebrafish larvae and juveniles were in accordance with the Directive 2010/63/EU of the European Parliament and the Council of the European Union and approved by the Norwegian Food Safety Authorities.

METHOD DETAILS

Two-photon calcium imaging

For *in vivo* imaging, fish were embedded in 2-2,5% low-melting-point agarose (LMP, Fisher Scientific) in a recording chamber (Fluorodish, World Precision Instruments). To ensure odor to arrive to the nostrils, the LMP agarose was removed carefully in front of the nose, after solidifying for 20min. The constant perfusion of AFW bubbled with carbogen (95% O_2 and 5%CO_2) was maintained during the experiment.

For *in vitro* imaging, brain explants were prepared as described in section "Dissection of juvenile zebrafish brain explant" below. The preparation is constantly perfused with artificial cerebrospinal fluid (ACSF). ACSF was bubbled with carbogen (95% O_2 and 5% CO_2) throughout the experiment.

Two-photon microscopes were used for calcium imaging: Scientifica, with a 16x water immersion objective; Nikon, NA 0.8, LWD 3.0 and Zeiss 7 MP with a 20x water immersion objective W Plan-Apochromat, NA 1.0. For excitation a mode-locked Ti:Sapphire laser (MaiTai Spectra-Physics) was tuned to 920nm. Recordings were performed as either single plane or volumetric recording (6-8 planes with a Piezo (Physik Instrumente (PI)). The acquisition rate was 6,4Hz for single plane recordings (image size 256x512 pixels) and between 2.3-3.4Hz per plane for volumetric scans (average image size 1536x750).

Odor preparation

Our odor panel consisted of food odor (1g/50ml dilution), skin extract (1g/50ml dilution), urea (10^{-4} M), bile-acid mixture (taurocholic acid, taurodeoxycholic acid at $5x10^{-4}$ M), amino acid mixture (Alanine, Phenylalanine, Methionine, Histidine, Cysteine, Arginine, Glutamic acid at 10^{-4} M), and ammonium chloride (10^{-4} M). All odorants were purchased from Sigma Aldrich. Food odor was prepared using commercially available fish food; 1g of food particles was incubated in 50ml of fish water (FW) for at least 1 h, filtered through filter paper, and diluted to 1:50. For skin extract,[97] adult zebrafish were first euthanized in ice-cold water and decapitated, the skin was peeled off from the body. 1g of skin was incubated in 2ml of AFW and was vortexed at 1300rpm for 1 h at 4°C. After, the skin extract was dissolved in 50ml of AFW and filtered through the filter paper. All odors were prepared from the frozen stocks immediately before use.

Odor delivery

The stimulation tube was positioned in front of the nose and the stimulus was delivered for 30 s. The stimulation was performed with HPLC injection valve (Valco Instruments) controlled with Arduino Due. Before each experiment, a trial with fluorescein (10^{-4}M in AFW) was performed to determine precise onset of odor delivery.

Micro-electrode stimulation

Electrodes were pulled from a borosilicate glass microcapillary (1.00 mm; World Precision Instruments) using a laser puller (Sutter Instruments Model P-2000). For single electrode stimulations (Figures 3 and 5), electrode tips were broken so that the final tip diameter of the stimulating electrode was around 10-15 μm. For dual electrode stimulations (Figures 4 and S4), high resistance (10-12MOhm) patch electrodes were used. The electrode was filled with artificial cerebro-spinal fluid (ACSF). Two-separate electrodes were connected to two poles of the ISO-flex stimulus isolator (A.M.P.I.), and electrodes were glued by two-component epoxy

so that the electrode tips are close to each other (within 1-2 mm). Only a single electrode tip was inserted and positioned in the brain explant using a micromanipulator (Scientifica, UK), and the other tip was left outside the brain. A train of 6 short current pulses (2-5 μA) for 50 ms duration and 20 s inter stimulus intervals was applied to the target brain region. For dual electrode stimulations, a train of 10 short current pulses (1 mA) for 2 ms duration and a inter stimulus interval of 60 s was applied to the first electrodes in the first target region, then followed by the same stimulus train for the other electrode in the next target region.

Dissection of juvenile zebrafish brain explant

All animals (3-4 weeks post fertilization) were anesthetized in ice-cold artificial fish water (AFW) and euthanized by decapitation in oxygenated (95% O_2/5% CO_2) artificial cerebro-spinal fluid (ACSF). The ACSF was composed of the following chemicals diluted in reverse osmosis–purified water: 131 mM NaCl, 2 mM KCl, 1.25 mM KH_2PO_4, 2 mM $MgSO_47H_2O$, 10 mM glucose, 2.5 mM $CaCl_2$, and 20 mM $NaHCO_3$.[97] Brain-explant dissections and experiments were was carried out in ACSF, bubbled 95% O_2/5% CO_2. After removing jaws and eyes, muscle tissue, gills and fat were cleaned to allow oxygen diffusions to the brain explant. Next, the skin tissue, bone and dura mater covering the forebrain was removed from the dorsal side, allowing electrode access.

QUANTIFICATION AND STATISTICAL ANALYSIS

Two-photon microscopy images were aligned using a method described in Reiten et al. and Diaz Verdugo et al.[55,56] Recordings were then visually inspected for remaining motion and Z-drift, recordings with remaining motion artifacts were discarded. Regions of interest (ROIs) corresponding to neurons were automatically detected using a template matching algorithm,[30,56] and visually confirmed. To calculate the time course of each neuron, pixels belonging to each ROI were averaged over time. For each ROI, fractional change in fluorescence (ΔF/F) relative to baseline was calculated.

Neurons were clustered into functional clusters using k-means clustering algorithm in MATLAB (Figures 1A, 2B, and 3E).[30] For Figure 2 an average activity of all neurons in each cluster of the habenula was averaged. This population vector was used as a reference activity and correlated with each neuron in the telencephalon.

Delineation of brain regions in the telencephalon was done manually on the raw image of the brain (as in Figure 2E) based on anatomical landmarks described in previous studies in zebrafish and other teleost fish.[66,76–78,80,95]

To identify optimal number of k-means clusters in the habenula and in the rest of forebrain, we used elbow-method.[98] First, the distance of each cluster element to the centroid of that specific cluster was calculated, and this value was normalized by distances from each cluster element to every centroid. This operation is iterated for 1-30 number of cluster number 'ks' (Figure S1B, black traces), and compared to shuffled/simulated data with same mean and variance, but no clustering (Figure S1B, gray traces), and subtracted to find the peak distance between real data and simulated data with no clusters, to reveal the optimal clusters number (Figure S1C). These analyses revealed that ongoing habenular activity can be optimally represented by 5-6, which we choose to use in our analysis. In addition to identifying optimal number of clusters, we also further verified that our key results are consistent even at multiple iterated numbers of clusters (Figure S1E).

Cluster selectivity was calculated to quantify the overlap of manually delineated brain regions with functional clusters of neurons identified using k-means clustering based on their spontaneous activity. Cluster selectivity index is the life-time sparseness[30] for the distribution of neurons within an anatomically defined brain region across the k-means clusters. If cluster selectivity is 1, it means that neurons of an anatomically identified brain region belong to one functional cluster. If cluster selectivity is 0, all neurons of an anatomically identified brain region are equally distributed into all functional k-means clusters.

Cluster fidelity was calculated by measuring the probability of pairs of neurons being in the same cluster during two different time periods.[30] We compared the cluster fidelity of real k-means clusters with shuffled the cluster identities of same neurons. We also verified that cluster fidelity of habenular neurons are stable across time, by calculating cluster fidelity across 10 consecutive 2.2 min time periods across 22 min of stable recording period (Figure S1D).

Across this paper, neurons were considered as responsive (to odor or forebrain stimulation) if their response (5 s) exceeded 2 standard deviations above the 5 s-baseline period preceding the stimulation. To calculate how odor and micro-stimulation influenced each other, we compared whether these two different stimuli can significantly (using Wilcoxon signed rank test) change each other when delivered simultaneously (odor + micro-stimulation).

In Figure 6, odor responses of habenular neurons were sorted by correlating their odor response with a step function, as previously described in Cheng et al.[18] Top 5% of habenular neurons with highest or lowest correlations were considered as strongly excited or inhibited, respectively. Averaged ongoing activity preceding the stimulation in those classified habenular neurons was used as a reference vector and correlated with each forebrain neuron to identify forebrain neurons that are highly correlated with excited or inhibited habenular neurons.

Statistics

Statistical analysis was done using MATLAB; p values are represented in the figure legends as (*$p < 0.05$, **$p < 0.01$, ***$p < 0.001$). Wilcoxon ranksum test was used for non-paired comparisons and Wilcoxon signed rank test for paired comparisons. All analysis was performed with Fiji and MATLAB.

Current Biology, Volume *31*

Supplemental Information

Ongoing habenular activity is driven by forebrain networks and modulated by olfactory stimuli

Ewelina Magdalena Bartoszek, Anna Maria Ostenrath, Suresh Kumar Jetti, Bram Serneels, Aytac Kadir Mutlu, Khac Thanh Phong Chau, and Emre Yaksi

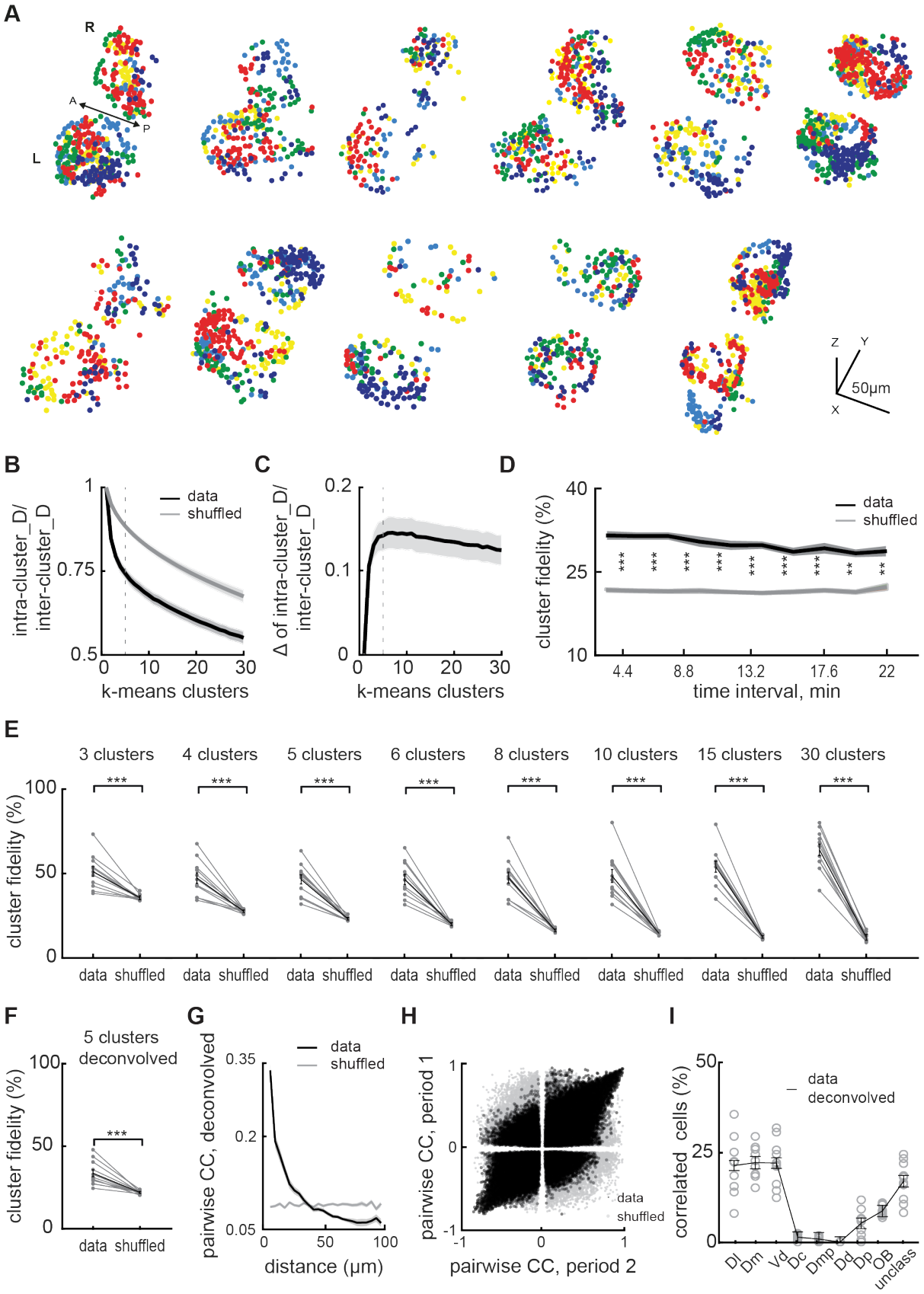

Figure S1. Functional clusters of habenular neurons are robust and stable across time. Related to Figures 1 and 2.

(A) Three-dimensional reconstructions of functional clusters of habenular neurons identified using k-means clustering in n=11 zebrafish. Functional clusters of neurons with similar ongoing activity are color-coded into 5 clusters. Colors are arbitrarily assigned by clustering algorithm, but manually matched across animals L-left; R-right hemisphere, A-anterior, P-posterior.

(B) Identification of optimal number of clusters by using elbow analysis. Elbow analysis calculate the sum of intra-cluster distances "D" of each cluster element, normalized by sum of average inter-cluster distances of each cluster element, for actual data (black), and for simulated data (100 iterations) with the same variance of actual data but with no cluster structure (grey), in n=11 zebrafish. This calculation is repeated for up to 30 clusters (x-axis). Optimal number of clusters is the elbow point, where the black curve shows a prominent bend. Dashed lines marks k-means analysis for 5 clusters. Shaded bars are SEM.

(C) Optimal number of clusters is further revealed, when actual data is compared to simulated data with similar variance but no cluster structure, by taking the difference of two curves in (B). Note that the peak point of this difference reveals 5-6 optimal number of clusters in ongoing habenular activity. 5 clusters were chosen to be used in k-means analysis of habenular activity in this paper for keeping the color scheme simple and easy to visualize.

(D) Stability of habenular clusters is investigated by calculating cluster fidelity of neurons (mean ± SEM) in the first 2.2 minute in comparison to consecutive 2.2 minute time bins, in real data (black), and in simulated data with shuffled cluster identities (100 iterations, in grey). Note that while cluster fidelity remains stable (around 40%, and with no significant change across consecutive time points), simulated data with shuffled cluster identities shows low cluster fidelity across time. Real data always remain significantly higher than shuffled control. Shaded bars are SEM. (*$P < 0.05$, **$P < 0.001$, ***$P < 0.001$, Wilcoxon signed-rank test).

(E) Cluster fidelity calculated for k-means analysis using multiple number of clusters. Note that for all numbers of k-means clusters, cluster fidelity remains significantly higher than control data with shuffled cluster identities. (***$P < 0.001$, Wilcoxon signed-rank test).

(F) Cluster fidelity is calculated for 5 k-means clusters, using temporally deconvolved calcium signals of habenular activity. (***$P < 0.001$, Wilcoxon signed-rank test).

(G) Relation between pairwise correlation of habenular neurons and the distance between each neuron pair is calculated using temporally deconvolved calcium signals of habenular activity.

(H) Pairwise correlations of habenular neurons during two consecutive time periods, calculated using temporally deconvolved calcium signals of habenular activity (black). Control pairwise comparison that are shuffled for pair identities (grey).

(I) Distribution of forebrain neurons with strong correlation (>0.1) to ongoing habenular activity into anatomically identified forebrain regions. Same as Figure 2G, but calculated using temporally deconvolved calcium signals. Note that results look similar for (G), (H), and (I) using calcium signals versus temporally deconvolved calcium signals.

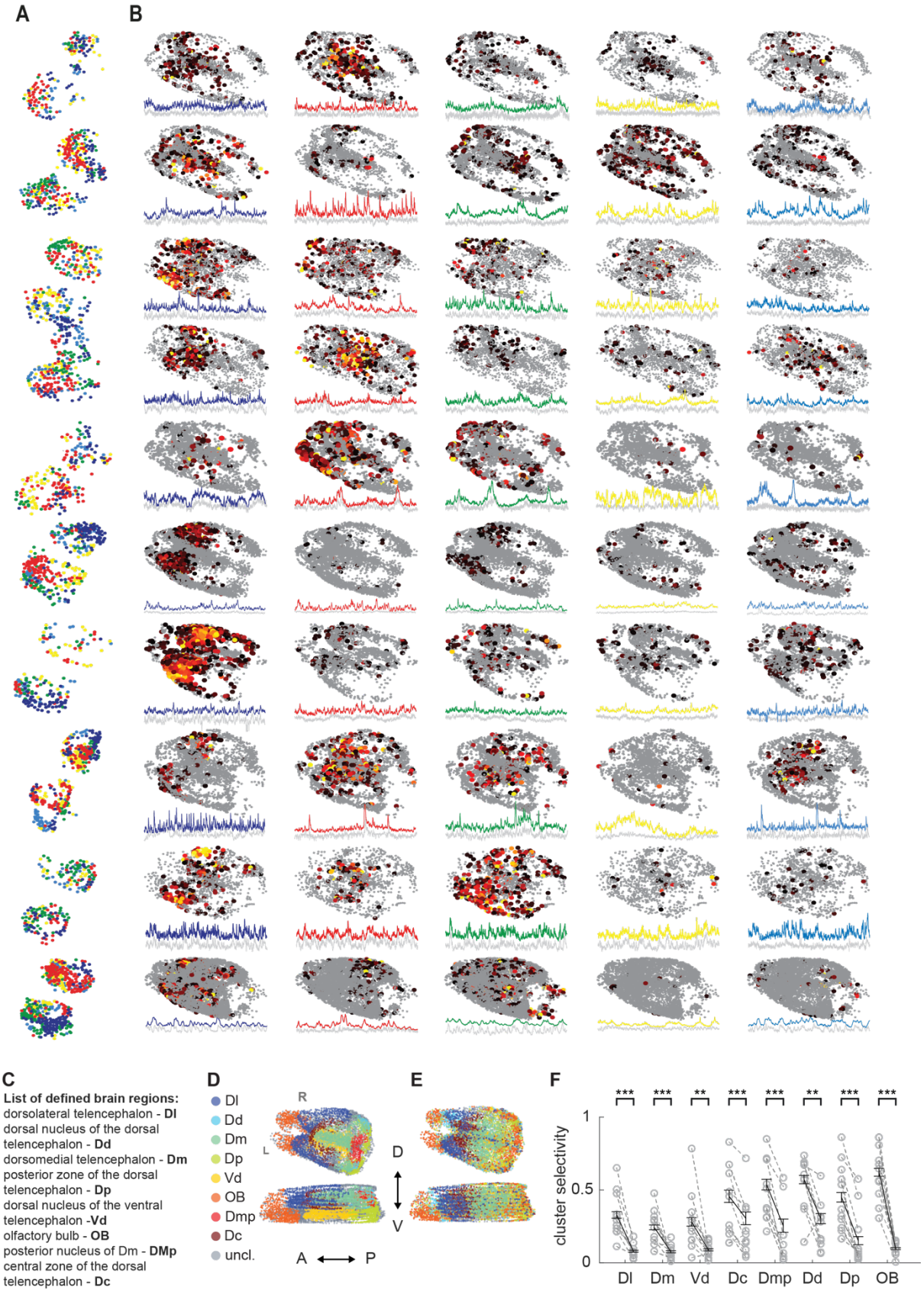

Figure S2. Functional and anatomical comparison of forebrain habenula interactions. Related to Figure 2.

(A) Three-dimensional reconstruction of habenular neurons detected in *Tg(elavl3:GCaMP6s)* zebrafish line, clustered with k-means clustering. Colors represent neural clusters with similar ongoing activity. L-left; R-right hemisphere. 315 ± 35 (mean ± SEM) habenular neurons were imaged in each fish (n=11 fish).

(B) Three-dimensional reconstruction of forebrain neurons that are strongly correlated (Pearson's correlation >0.1) to average ongoing activity of different habenular clusters in B. Warm colors represent stronger correlations. 2135 ± 345 (mean ± SEM) forebrain neurons were imaged in each fish (n=11 fish). Color-coded traces represent the average activity of forebrain neurons in each cluster. Grey traces represent the average activity of corresponding habenular clusters in A. Note that the ongoing activity of identified forebrain neurons and habenular clusters are highly similar.

(C) A list of anatomically identified zebrafish forebrain regions and their abbreviations.

(D) Three-dimensional reconstruction of forebrain neurons identified by using anatomical landmarks. Top – dorsal view, bottom – coronal view. L-left; R-right hemisphere. A –anterior, P – posterior, D- dorsal, V-ventral. Colors corresponds to individual forebrain regions in C.

(E) Three-dimensional reconstruction of forebrain neurons that are clustered by k-means functional clustering (with n=8 clusters) of their ongoing neural activity. Each arbitrary color represents functional forebrain cluster.

(F) Neurons of anatomically identified forebrain regions exhibit cluster selectivity that are significantly higher than chance levels.

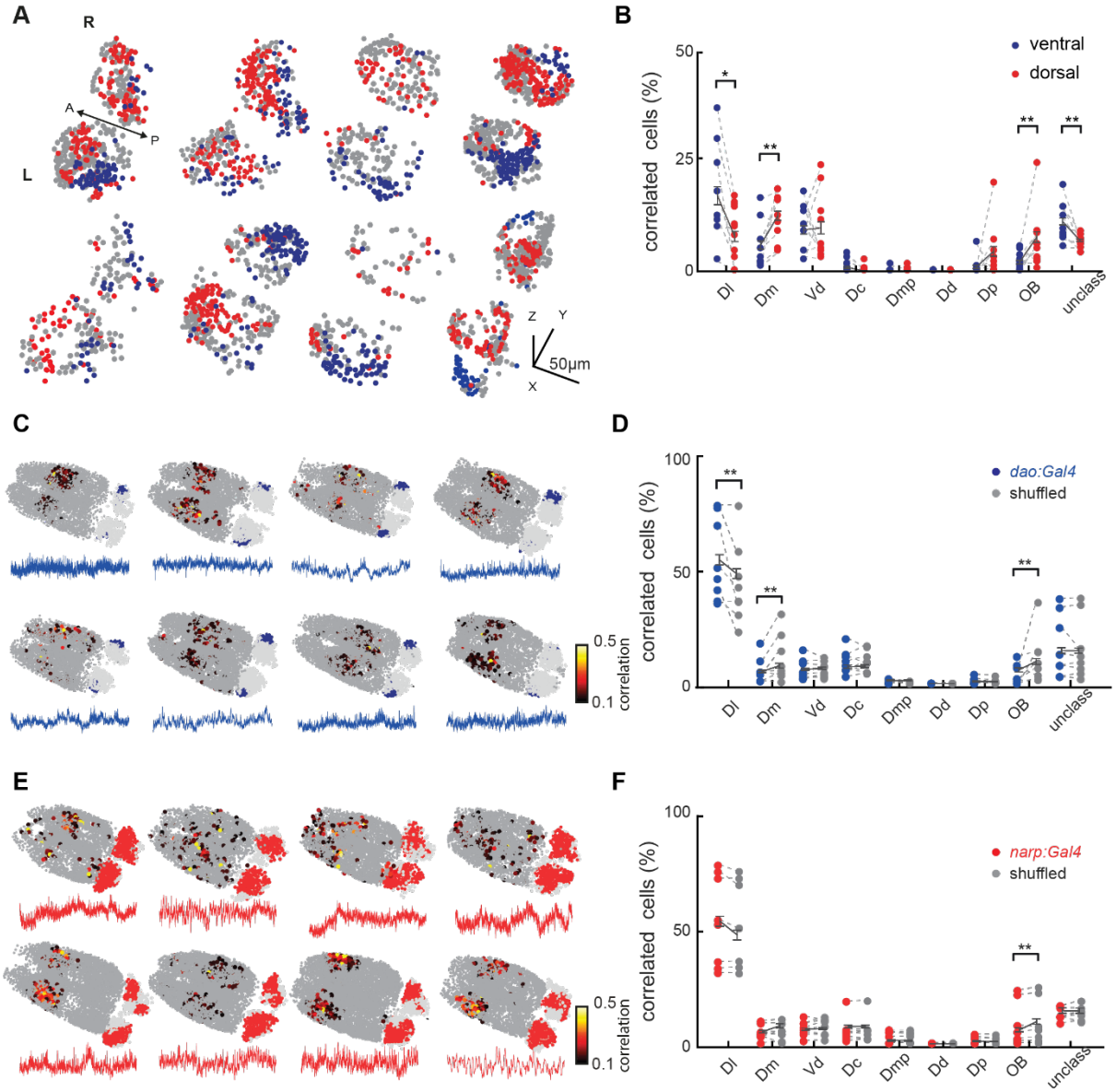

Figure S3. Ongoing activity of ventral and dorsal habenular neurons correlate preferentially with different forebrain regions. Related to Figure 2.

(A) Three-dimensional reconstruction of functional clusters in habenula corresponding to ventral (blue) and dorsal (red) zones of habenula in 11 *Tg(elavl3:GCaMP6s)* zebrafish.

(B) Anatomical distribution of forebrain neurons with strong correlation (>0.1) to ongoing activity of ventral (blue) versus dorsal (red) functional clusters of the habenula. Note that the functional clusters of neurons in ventral zones of the habenula shows significantly higher fraction of correlated neurons in Dl. Also note that the functional clusters of neurons in dorsal zones of the habenula shows significantly higher fraction of correlated neurons in Dm, Dp, OB and unclassified neurons across the forebrain. (*P < 0.05, **P < 0.01, Wilcoxon signed-rank test).

(C) Three-dimensional reconstruction of forebrain neurons in *Tg(elavl3:GCaMP6s); Tg(dao:GAL4VP16; UAS-E1b:NTR-mCherry)* zebrafish, which genetically labels vHb neurons (blue), in 8 zebrafish. Individual forebrain neurons with strong correlation (>0.1) to vHb are highlighted with warm colors. Non-correlated

forebrain neurons are in grey. Average ongoing activity of vHb neurons are plotted under each brain.

(D) Anatomical distribution of forebrain neurons with strong correlation (>0.1) to the average ongoing activity of genetically labelled vHb neurons (blue) versus similar number of randomly selected other habenular neurons (grey). Note that the vHb shows significantly higher fraction of correlated neurons in Dl, and significantly smaller number of correlated neurons in Dm and OB. (**P < 0.01, Wilcoxon signed-rank test).

(E) Three-dimensional reconstruction of forebrain neurons in *Tg(elavl3:GCaMP6s); Tg(narp:GAL4VP16; UAS-E1b:NTR-mCherry)* zebrafish, which genetically labels neurons in 68% of habenula, in 8 zebrafish. Individual forebrain neurons with strong correlation (>0.1) to *narp:GAL4VP16* labelled neurons are highlighted with warm colors. Non-correlated forebrain neurons are in grey. Average ongoing activity of vHb neurons are plotted under each brain.

(F) Anatomical distribution of forebrain neurons with strong correlation (>0.1) to the average ongoing activity of *narp:GAL4VP16* labelled neurons (blue) versus similar number of randomly selected other habenular neurons (grey). Note that the *narp:GAL4VP16* labelled dorsal habenular neurons do not show any significant preference of correlations in the forebrain, except the OB. (**P < 0.01, Wilcoxon signed-rank test).

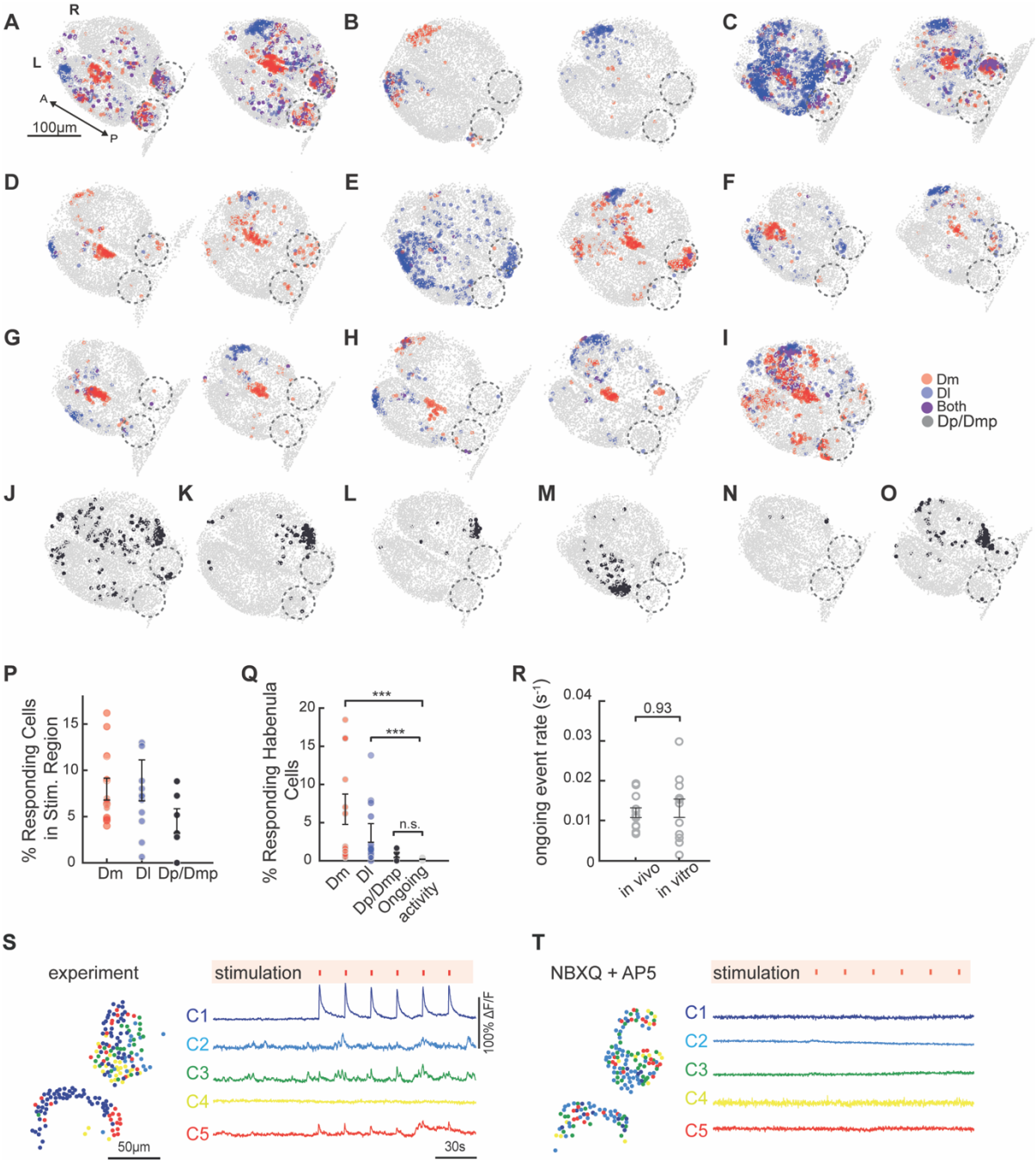

Figure S4. Three dimensional reconstructions of all micro-electrode stimulations in zebrafish forebrain. Related to Figures 3 and 4.

(A-I) All three-dimensional forebrain reconstructions in *Tg(eval3:GCaMP6-nuclear)* juvenile zebrafish brain explant, upon sequential Dm and Dl stimulations. Each panel represents an individual fish. Neurons responding to only Dm (red), only Dl (blue), both (magenta) stimulations, and non-responsive (grey). Scale bar 100µm, L-left; R-right; A-anterior; P-posterior.

(J-O) All control stimulations upon inserting micro-electrode to regions near Dp/Dmp. Each panel represents an individual fish. Neurons responding to Dp/Dmp stimulation (black), non-responsive (grey). Habenulae are delineated by dashed black circles.

(P) Fraction of forebrain neurons in Dm, Dl and Dp/Dmp regions activated by (above 2SDs) to the micro-electrode stimulation of these specific brain regions. No significant differences were observed in the fraction of neurons activated in these brain regions.

(Q) Fraction of habenular neurons responding to Dm, Dl and Dp/Dmp stimulation (black), when compared to randomly selected periods of ongoing habenula activity (grey). Habenular ongoing activity periods was selected from 100 random time points. Note that while Dm and Dl activation recruits habenular neurons significantly more than random periods of ongoing habenular activity different (***$P < 0.001$, Wilcoxon ranksum test), this is not the case for control stimulations of Dp/Dmp region.

(R) Frequency of ongoing calcium events detected in vivo versus brain-explant preparation. Note that no significant difference was observed between these two preparations (Wilcoxon ranksum test).

(S) Left, representative example of habenular neurons detected in Tg(eval3:GCaMP5) zebrafish line during forebrain micro-stimulation, clustered with k-means clustering. Neurons are color-coded based on their cluster identity (C1-5). Right, average activity of each habenular functional cluster (colors corresponds to panel A) during 6 consecutive, 50ms forebrain micro-stimulations. Clusters are defined by k-means clustering. Forebrain micro-stimulations are marked in red.

(T) Same example fish in (S), but after the bath application of AMPA+NMDA receptor blockers, NBXQ(5μm) + AP5(25μm). Note that in the presence of AMPA+NMDA receptors blockers, no habenular responses are detected

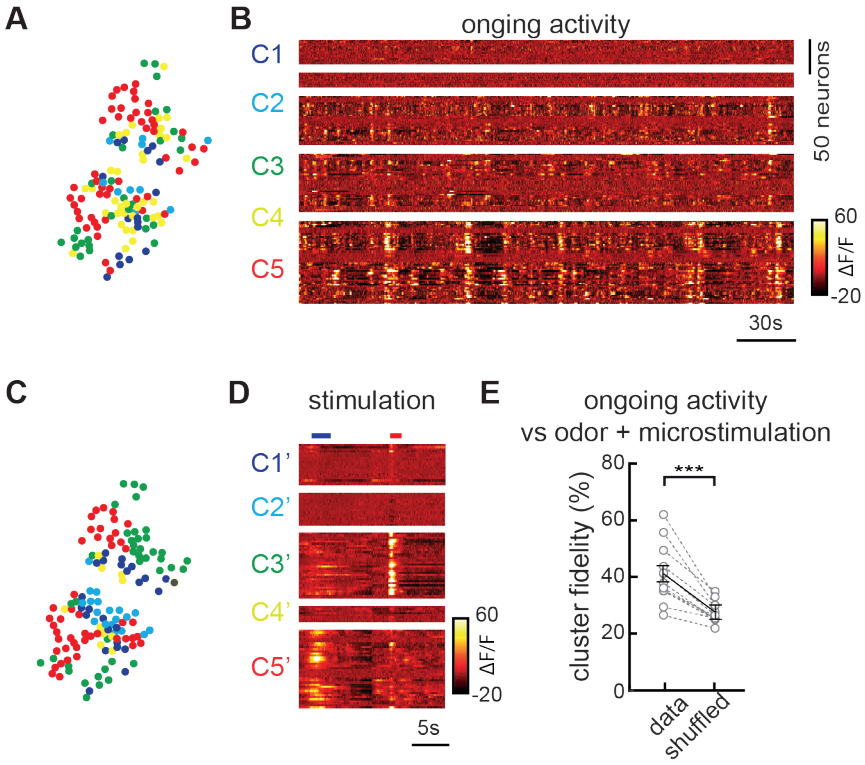

Figure S5: Cluster identities of habenular neurons remains stable during forebrain and odor stimulation. Related to Figure 5.

(A) Representative example of habenular neurons clustered with k-means functional clustering of their ongoing activity in juvenile zebrafish brain explant. Colors represent habenular clusters with similar ongoing activity.

(B) Ongoing activity of the habenular neurons corresponding to clusters in A.

(C) Representative example of habenular neurons clustered during forebrain and odor stimulation using k-means clustering. Colors represent habenular clusters with similar responses to forebrain micro-stimulation and odor stimulation. Note the similarity of clusters in A and C.

(D) Forebrain micro-stimulation and odor responses of the habenular neurons corresponding to clusters in C. Blue line indicates odor stimulation, red – micro-stimulation.

(E) The ratio of habenular neuron pairs remaining in the same functional clusters (cluster fidelity) is significantly higher than chance levels, during ongoing activity and forebrain and odor stimulation. ***$p<0.001$, Wilcoxon signed rank test.

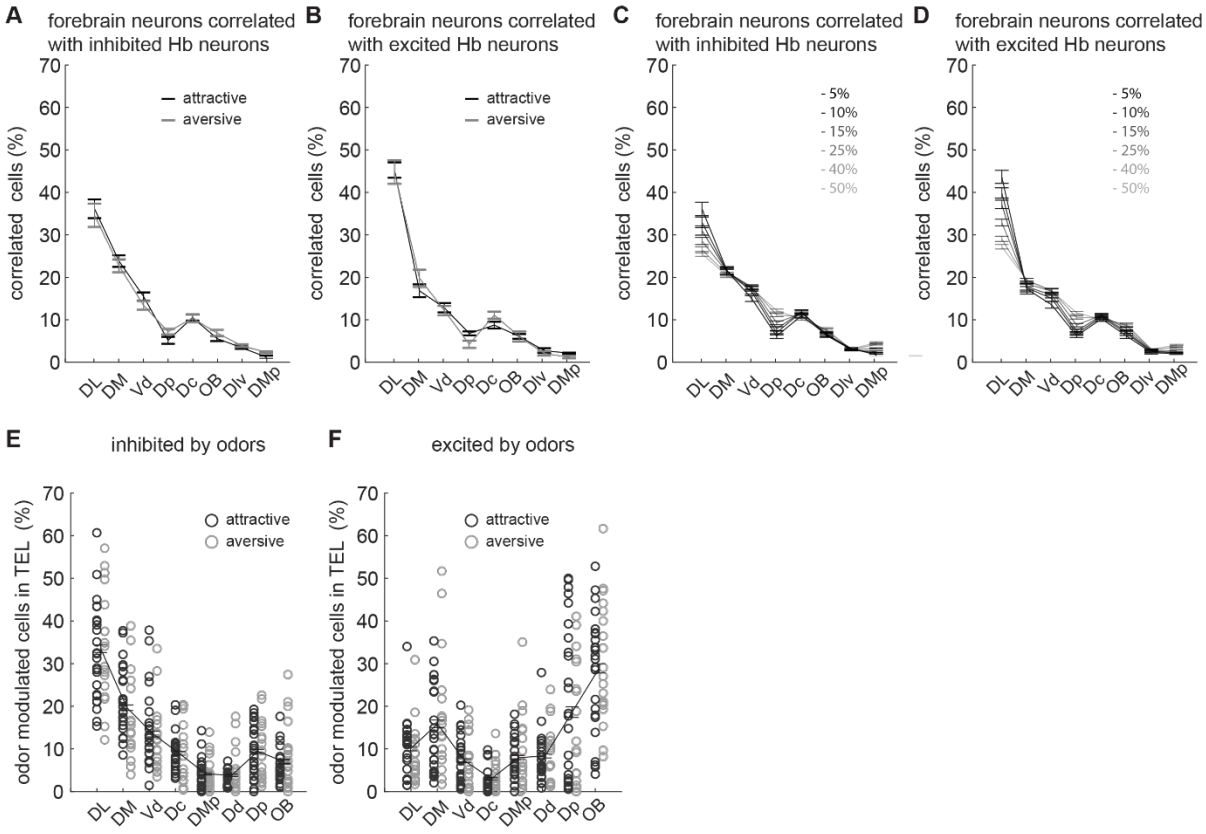

Figure S6. Distribution of forebrain neurons into anatomically identified forebrain regions, based on their odor responses, or their synchrony with odor modulated habenular neurons. Related to Figure 6.

(A) Anatomical distribution of forebrain neurons that are correlated with habenular neurons (top 5%) that are inhibited by odors in 10 fish.

(B) Anatomical distribution of forebrain neurons that are correlated with habenular neurons (top 5%) that are excited by odors in 10 fish. In A and B, attractive odors are in black, aversive odors are in grey. Lines represent mean ± SEM.

(C) Anatomical distribution of forebrain neurons with varying threshold for strong correlations (between top 5 and 50%) to ongoing activity of habenular neurons that are inhibited by odors in n=10 fish. Related to Figure 6E.

(D) Anatomical distribution of forebrain neurons with varying threshold for strong correlations (between top 5 and 50%) to ongoing activity of habenular neurons that are excited by odors in n=10 fish. Related to Figure 6E.

(E) Anatomical distribution of forebrain neurons that are most (top 5%) inhibited by odors in 10 fish. Black and gray circles represent attractive and aversive odors, respectively. Black lines represent mean ± SEM.

(F) Anatomical distribution of forebrain neurons that are most (top 5%) excited by odors in 10 fish. Black and gray circles represent attractive and aversive odors, respectively. Black lines represent mean ± SEM. Dl – dorsolateral telencephalon, Dd – dorsal nucleus of the dorsal telencephalon, Dm – dorsomedial telencephalon, Dp – posterior zone of the dorsal telencephalon, Vd – dorsal nucleus of the ventral telencephalon, OB – olfactory bulb, Dmp – posterior nucleus of dorsomedial telencephalon, Dc – central zone of the dorsal telencephalon.